

Hubble Space Telescope survey of the Perseus cluster – IV. Compact stellar systems in the Perseus cluster core and ultracompact dwarf formation in star-forming filaments

Samantha J. Penny,^{1,2,3*} Duncan A. Forbes³ and Christopher J. Conselice⁴

¹*School of Physics, Monash University, Clayton, Victoria 3800, Australia*

²*Monash Centre for Astrophysics, Monash University, Clayton, Victoria 3800, Australia*

³*Centre for Astrophysics and Supercomputing, Swinburne University of Technology, Hawthorn, Victoria 3122, Australia*

⁴*School of Physics and Astronomy, University of Nottingham, Nottingham NG7 2RD*

Accepted 2012 February 1. Received 2012 January 31; in original form 2011 December 18

ABSTRACT

We present the results of the first search for ultracompact dwarfs (UCDs) in the Perseus cluster core, including the region of the cluster around the unusual brightest cluster galaxy NGC 1275. Utilizing *Hubble Space Telescope* Advanced Camera for Surveys imaging, we identify a sample of 84 UCD candidates with half-light radii $10 < r_e < 57$ pc out to a distance of 250 kpc from the cluster centre, covering a total survey area of ~ 70 arcmin². All UCDs in Perseus lie in the same size–luminosity locus seen for confirmed UCDs in other regions of the local Universe. The majority of UCDs are brighter than $M_R = -10.5$, and lie on an extrapolation of the red sequence followed by the Perseus cluster dwarf elliptical population to fainter magnitudes. However, three UCD candidates in the vicinity of NGC 1275 are very blue, with colours $(B - R)_0 < 0.6$ implying a cessation of star formation within the past 100 Myr. Furthermore, large blue star clusters embedded in the star-forming filaments are highly indicative that both proto-globular clusters (GCs) and proto-UCDs are actively forming at the present day in Perseus. We therefore suggest star-forming filaments as a formation site for some UCDs, with searches necessary in other low-redshift analogues of NGC 1275 necessary to test this hypothesis. We also suggest that tidal disruption of dwarf galaxies is another formation channel for UCD formation in the core of Perseus as tidal disruption is ongoing in this region as evidenced by shells around NGC 1275. Finally, UCDs may simply be massive GCs based on strong similarities in the colour trends of the two populations.

Key words: galaxies: clusters: general – galaxies: clusters: individual: Perseus cluster – galaxies: dwarf – galaxies: star clusters: general.

1 INTRODUCTION

Deep, space-based imaging using the *Hubble Space Telescope* (*HST*) has made it possible to study the cores of nearby rich clusters in incredible detail, including their compact stellar systems. The class of compact stellar systems includes globular clusters (GCs) and compact ellipticals (cEs) but had no comparable objects of intermediate luminosity or size, until the discovery of ultracompact dwarfs (UCDs) by Hilker et al. (1999) and Drinkwater et al. (2000). UCDs are typically defined to have sizes $10 < r_e < 100$ pc and luminosities of $-10.5 > M_V > -14$, whereas GCs have lower luminosities and near constant sizes of $R_h \sim 3$ pc and the prototype cE M32 has $R_h \sim 120$ pc and $M_V \sim -16.5$ (Kent 1987).

As sample sizes of compact stellar systems have increased and selection criteria relaxed, it has become clear that the boundaries between UCDs, GCs and other star clusters have become increasingly blurred (Price et al. 2009; Madrid et al. 2010; Brodie et al. 2011; Forbes & Kroupa 2011; Huxor et al. 2011). Thus it is important to fully sample the parameter space of size and luminosity (within a given surface brightness limit) to obtain a true census of the compact stellar systems in any cluster environment.

The origin and nature of UCDs are yet to be determined, with numerous hypotheses put forward to explain the origin of these objects. The simplest explanation for the origin of UCDs is that they are an extension of GCs to higher magnitudes and sizes. Evidence for this exists in their colours, with UCDs lying along the red and blue subpopulations of the GC colour–magnitude trend. These objects also follow a similar spatial distribution as the GC system of their host galaxy (Mieske et al. 2008; Gregg et al. 2009). The

*E-mail: samantha.penny@monash.edu

larger masses of UCDs might be reached via the mergers of GCs (Fellhauer & Kroupa 2002; Kissler-Patig, Jordán & Bastian 2006). Therefore uncovering the true nature of UCDs requires not only the study of these bright, massive star clusters but also the GC system of the environment in which they reside.

Given UCDs are primarily found in relatively high-density regions of the Universe such as clusters, they might be formed during mergers between gas-rich galaxies (Fellhauer & Kroupa 2002; Brüns et al. 2011). When these galaxies interact, colliding gas clouds will be compressed enough to form stars in superclusters with masses 10^7 – $10^8 M_{\odot}$ with sizes ~ 100 pc. Some of these superclusters will undergo mergers, resulting in long-lived, compact objects that survive to the present day as UCDs.

Alternatively, it has been hypothesized that UCDs could be the nuclear star clusters of dwarf galaxies stripped via tidal interactions (Bekki, Couch & Drinkwater 2001; Drinkwater et al. 2003). Because of the dense nature of clusters, encounters between dwarf and massive galaxies would be expected to be commonplace. After several passages around their host cluster or galaxy, the dwarf may be completely stripped of its stellar envelope, with only the dense nucleus remaining. The cores of rich clusters are extremely high-density environments, where the strong cluster tidal potential would be hazardous to any object not sufficiently massive to withstand its influence (Penny et al. 2009).

Uncovering the origin of these objects requires searches in all environments, from isolated galaxies to the cores of the densest galaxy clusters. The identification of UCDs is confined to the local Universe ($D < 100$ Mpc), and must be carried out with high-resolution, space-based imaging due to the small physical and, therefore, small angular sizes of these objects. Compact stellar systems have been studied in many nearby clusters of galaxies. These include the following: Virgo at 16.5 Mpc (Hasegan et al. 2005; Evstigneeva et al. 2007; Brodie et al. 2011); Fornax at 19 Mpc (Hilker et al. 1999; Drinkwater et al. 2000; Gregg et al. 2009); Antlia at 35 Mpc (Smith Castelli et al. 2008); Centaurus at 45 Mpc (Mieske et al. 2009; Misgeld, Hilker & Mieske 2009); Hydra I at 47 Mpc (Wehner et al. 2008; Misgeld et al. 2011) and Coma at 100 Mpc (Price et al. 2009; Madrid et al. 2010; Chiboucas et al. 2011). A notable exception is the Perseus cluster at a distance of 71 Mpc.

This is the first search for UCDs in the Perseus cluster. At a redshift $z = 5366 \text{ km s}^{-1}$ (Struble & Rood 1999), and distance $D = 71$ Mpc, the Perseus cluster (Abell 426) is one of the nearest rich galaxy clusters, some 30 Mpc closer than the more frequently studied Coma cluster. Perseus has a very low spiral galaxy fraction in its core, with the majority of its members being elliptical and S0 galaxies. Given its proximity and richness, it represents an ideal location to identify compact stellar objects. However, due to its low Galactic latitude ($b = -13^{\circ}$), it has not been studied in as much detail as other clusters such as Virgo and Coma.

The Perseus cluster is furthermore an interesting target for the identification of UCDs due to its highly unusual brightest cluster galaxy (BCG) NGC 1275. NGC 1275 is clearly not a simple system, and exhibits a highly complex structure, including an extended system of filaments. Along the line of sight, there are two systems (Minkowski 1955): the high-velocity system at $V = 8200 \text{ km s}^{-1}$ falling towards the centre of the cluster, and a low-velocity system at $V = 5200 \text{ km s}^{-1}$. A massive, extended system of emission line nebulae extends from the nucleus of the low-velocity system. A number of filaments are seen that contain young, blue star-forming regions, which deserve investigation as sites of ongoing massive star cluster formation at the present time in the local Universe.

We carry out a search and analysis of compact stellar systems in the Perseus cluster of galaxies, utilizing high-resolution *HST* Advanced Camera for Surveys (ACS) Wide Field Channel (WFC) imaging in the *F555W* and *F814W* bands. In addition to this data, we also use archival ACS data in the *F435W* and *F625W* bands to search for UCDs in the vicinity of the cluster-centred galaxy NGC 1275.

In Section 2 we describe our data set, with the analysis described in Section 3. The sizes, colour and properties of the UCDs we identify in our imaging are presented in Section 4. We examine the GC populations of the BCG NGC 1275 and the giant elliptical NGC 1272 in Section 5. A discussion of our results including formation scenarios for these objects is presented in Section 6, with our conclusions in Section 7.

Throughout this paper we adopt $D = 71$ Mpc as the distance to the Perseus cluster, corresponding to an angular scale of 1 arcsec = 0.36 kpc. All the UCDs and GCs we identify in Perseus are at this time candidates as we do not yet have spectroscopic redshifts to confirm their cluster membership. All sizes presented in the paper for UCDs and GCs are effective (half light) radii.

2 DATA

2.1 ACS imaging

We have obtained *HST* ACS WFC imaging in the *F555W* and *F814W* bands for five fields in the core of the Perseus cluster. The exposure times were one orbit (~ 2200 s) per band per field. The scale of these images is $0.05 \text{ arcsec pixel}^{-1}$, and the ACS WFC field of view is $202 \times 202 \text{ arcsec}^2$. This results in a survey area of $\sim 57 \text{ arcmin}^2$ in *V* and *I*, out to a distance of ~ 250 kpc from the cluster centre (taken to be NGC 1275). These observations cover the giant elliptical NGC 1272 along with four other fields, but exclude the cluster-centred galaxy NGC 1275. Six fields were targeted originally, but due to a guide star acquisition failure, observations of one of the fields located at $\alpha = 03:19:25.95$, $\delta = +41:25:33.9$ (J2000.0) were not possible.

Data covering the cluster-centred galaxy NGC 1275 (Perseus A) are taken from the *HST* data archive. The imaging was obtained in the *F435W* and *F625W* bands, corresponding to *B* and *R*, respectively. The total exposure times used in this paper are 4962 s in *R*, and 4917 s in *B*. These observations are also drizzled to a scale of $0.05 \text{ arcsec pixel}^{-1}$. The resulting seven ACS fields that were successfully targeted are shown in Fig. 1 and listed in Table 1.

3 DATA ANALYSIS

3.1 Object identification

We identify objects in our imaging using *SExtractor* (Bertin & Arnouts 1996). Bright ellipticals were subtracted from our images prior to the object detection. Elliptical isophote fitting of these galaxies was done using the *IRAF* task *ELLIPSE*. Model galaxies were then created using the *IRAF* routine *BMODEL*, with the task *IMARITH* used to subtract these models from the original imaging. This subtraction reveals a large compact star cluster population which would otherwise have been missed during object identification via *SExtractor*. This population may include potential UCD candidates.

The complex nature of NGC 1275 makes the subtraction of this galaxy via ellipse fitting very difficult. The presence of a saturated nucleus, dust lanes and filaments resulted in a poor subtraction of the underlying galaxy, with the dust lanes obscuring many GCs in

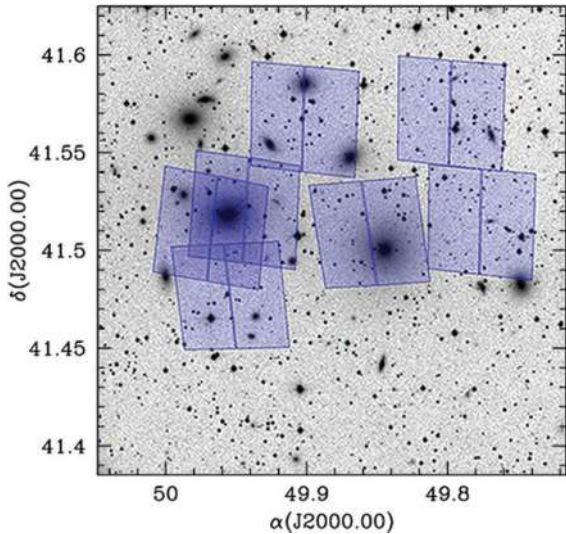


Figure 1. The regions of the Perseus cluster core covered in this study. The highlighted regions represent the seven ACS WFC fields ($202 \times 202 \text{ arcsec}^2$). The two brightest galaxies are visible to the centre left (NGC 1275) and centre right (NGC 1272) of the image. NGC 1275 itself is covered by two overlapping pointings. The survey area for the rest of the cluster is not contiguous, but was rather designed to target dEs visible in ground-based imaging whilst avoiding very bright stars.

these central regions. Likewise, removing the galaxy’s light via the subtraction of a smoothed version of the image (unsharp masking) would leave the extensive dust lanes and other substructure behind, obscuring a large central region of the galaxy. The presence of dust would furthermore lead to large uncertainties in the colours of central star clusters. Therefore we decided not to remove this galaxy from the original image. As a result, the study of this particular region of the cluster excludes the inner 6-kpc region of NGC 1275.

Objects were identified in the galaxy subtracted images using SExtractor, with photometry performed on the original, non-galaxy subtracted images. We identified all objects at least 5 contiguous pixels in size at 3σ above the noise level independently in both bands, and then matched the catalogues. This catalogue matching ensures that objects detected in only one band (e.g. cosmic rays that were not properly cleaned) do not make it into our final catalogue, as would be the case if detection was carried out in one band only.

3.2 Photometry

The total magnitudes are measured using SExtractor ISOCOR. The flux of the object above a threshold level is measured, and then

Table 1. The seven *HST* ACS observations used in this paper. Their positions are shown in Fig. 1. Because of guide star acquisition failure, no data are available for the field Perseus cluster 2.

Field	α (J2000.00)	δ (J2000.00)	Filters
Perseus cluster 1	03:19:47.90	+41:28:00.2	<i>F555W</i> , <i>F814W</i>
Perseus cluster 3	03:19:23.17	+41:29:59.0	<i>F555W</i> , <i>F814W</i>
Perseus cluster 4	03:19:04.72	+41:30:10.8	<i>F555W</i> , <i>F814W</i>
Perseus cluster 5	03:19:34.57	+41:33:37.1	<i>F555W</i> , <i>F814W</i>
Perseus cluster 6	03:19:09.13	+41:33:49.9	<i>F555W</i> , <i>F814W</i>
NGC 1275 SE	03:19:51.01	+41:30:41.7	<i>F435W</i> , <i>F625W</i>
NGC 1275 SW	03:19:45.82	+41:30:41.5	<i>F435W</i> , <i>F625W</i>

a correction is made for the flux lost in the wings of the object, assuming the profile of the object is Gaussian. The background for each object is estimated locally as it varies across the field of view due to the presence of giant ellipticals and intracluster light. Colours are measured using fixed 3 pixel apertures centred on each object to ensure the same extent of the objects in both bands are being sampled in the colour calculation. The *F555W* and *F814W* magnitudes are then converted to *V* and *I*, respectively, using the transformations of Sirianni et al. (2005). Transformations are likewise applied to the *F435W* and *F625W* magnitudes to convert them to *B* and *R*.

Reddening corrections are then applied to our photometry. The Perseus cluster is at a low Galactic latitude, and lies in a region of variable extinction (Burstein & Heiles 1984). To check for any effects that this might have on the measured colours of our objects, we find the reddening corrections at the centres of each of our *HST* pointings using the extinction maps of Schlegel, Finkbeiner & Davis (1998). The values of $E(B - V)$ vary between 0.160 and 0.164 across our survey area, therefore, we choose not to vary our reddening corrections with cluster position. Our reddening corrections do not take into account internal extinction by NGC 1275, which contains patchy dust. The likely effect of reddening caused by the dust of NGC 1275 is discussed in Section 4.2. A colour–magnitude diagram constructed from the initial SExtractor catalogues reveals a large amount of foreground and background contamination, with a sequence of objects belonging to Perseus also visible.

3.3 Size measurements

Sizes for all objects were determined using the fitting code ISHAPE (Larsen 1999), which is commonly used to derive the shape parameters of objects that are only slightly resolved such as extragalactic GCs and UCDs (e.g. Harris 2009; Madrid et al. 2010). ISHAPE requires a model of the point spread function (PSF), and we describe the fitting of this PSF below.

3.3.1 Point spread function fitting

In order to determine the sizes of our objects using ISHAPE, we need to build the ACS PSF. Given the low Galactic latitude of Perseus ($b = -13^\circ$), numerous suitable stars are available in each field for which to fit the PSF, therefore, we build a separate PSF for each frame. The ACS PSF is built using the IRAF package DAOPHOT. The DAOPHOT task PSTSELECT was used to identify stars from which to construct the ACS PSF. Bright but non-saturated stars that are well isolated were then selected manually from the list provided by PSTSELECT with which to build the PSF. The PSF was computed with the task PSF, and then oversampled by a factor of 10 as required by ISHAPE.

3.3.2 Size determination

The PSF is then used in the determination of the sizes of our objects using ISHAPE. The effective radius, r_e , is determined for each object by fitting a PSF convolved profile to each object in the image. By varying the full width at half-maximum (FWHM) of the model profile, ISHAPE finds a best fit to the object using the given analytical model. We fit all objects using a King profile with a concentration parameter $c = 30$, as previous authors have found this to be the typical concentration parameter for GCs and UCDs across a range of locations. The fitted FWHM is then converted to an effective radius (containing half the object’s light) using the conversion

$r_e = 1.48 \times \text{FWHM}$ provided in the *ISHAPE* documentation for a King profile with a concentration parameter $c = 30$.

The fitting is performed on the original, non-galaxy subtracted imaging, and is effective down to ~ 10 per cent of the FWHM of the PSF (Harris et al. 2009). This corresponds to 0.2 pixels for ACS/WFC, which is 3.5 pc at the distance of Perseus. Objects must therefore have effective radii larger than 3.5 pc to be included in our final sample of star clusters with reliable size measurements. However, all objects with $r_e > 1$ pc (i.e. non-zero radii, or not stars) and signal-to-noise ratio (S/N) > 10 in both bands are included in plots showing both UCDs and GCs. All sizes presented in the paper for UCDs and GCs are effective radii.

There is a large foreground contamination of stars which need to be removed from our sample that at fainter magnitudes are visually indistinguishable from GCs and UCDs. *ISHAPE* typically fits stars with effective radii of zero, allowing for their easy removal from our sample. However, saturated stars will be fitted with non-zero sizes by *ISHAPE*, with flat-topped light distributions that do not follow the PSF. It is therefore essential that these objects are cleaned from our catalogue. Because of the fact that a point source (i.e. star) may saturate in one band but not the other, it would therefore be fit by *ISHAPE* with a non-zero FWHM in the saturated band. It follows that the radius of each object is checked in both the *F814W* and *F555W* bands to ensure our catalogues are properly cleaned of point sources. We therefore remove all objects that are saturated in at least one band. This check is likewise performed for the *F435W* and *F625W* imaging of the NGC 1275 region.

We make no selection cuts based on colour, size or ellipticity prior to running *ISHAPE* on the sample. Instead, our catalogues were cleaned via visual inspection of all objects after the *ISHAPE* fitting routine was run to remove spurious detections from our sample. Obvious bright background galaxies, edge objects, dwarf ellipticals (dEs), stars and other artefacts (such as diffraction spikes) are then removed by eye from the catalogue of objects successfully fitted by *ISHAPE*.

Compact star clusters are then identified in this catalogue. We define compact objects to have sizes $1 < r_e < 150$ pc with objects $r_e < 10$ pc classed as GCs, and compact objects larger than this taken to be UCDs. Thus we follow Brodie et al. (2011) in not imposing a luminosity criteria on UCDs. The upper size limit of 150 pc ensures background ellipticals do not make our final sample, with the largest UCD we identify having size $r_e = 57$ pc. The cleaned colour–magnitude diagrams for these two regions are shown in Fig. 2. Only compact objects are shown in this plot. This combination of manual cleaning and the removal of stars via PSF fitting using *ISHAPE* is highly successful, with clear colour sequences defined by the compact stellar systems.

At the distance of Perseus, a typical GC of $r_e = 2.5$ pc will be too small to have its size accurately determined by *ISHAPE*, as their effective radii will be less than 10 per cent of the ACS PSF. Therefore any compact objects we identify in this imaging with reliable sizes will be larger than 3.5 pc, and will be extended GCs or larger objects.

4 ULTRA COMPACT DWARFS

Identifying UCDs requires the measurements of their sizes, which necessitates their S/N to be sufficiently high for *ISHAPE* to determine accurate sizes. Therefore, to identify the minimum S/N at which sizes for compact objects can be accurately determined, we compare the sizes of objects > 3.5 pc in both bands as determined by *ISHAPE*

at different S/N thresholds. At low S/N (< 30), objects are typically not well matched in both bands, with a large scatter between the effective radii measured in the *F814W* and *F555W* bands. However, at $S/N > 40$ the sizes of the objects are in general well matched in both bands. We therefore select only those objects with a minimum S/N of 40 in the *F555W* band for our UCD identification, which is the shallower of the two bands. The same S/N criteria are applied to the *F435W* and *F625W* band imaging for NGC 1275.

UCDs typically have effective radii $10 < r_e < 150$ pc. To create our sample of candidate UCDs, objects must have sizes that fall in this range in both the *F814W* and *F555W* bands, and a minimum S/N of 40 in both bands. We follow Brodie et al. (2011) making no colour or luminosity selection criteria. All objects matching these criteria are then carefully examined in both the *F555W* and *F814W* imaging, and any objects missed in our initial cleaning with visually clumpy or galaxy-like substructure in either band are removed. Identical selection criteria are used to identify UCD candidates in the NGC 1275 region.

Cut-outs of all candidate UCDs in our imaging are shown in Figs 3 and 4, and their properties listed in Tables 2 and 3. This imaging shows that all UCDs we identify are round systems, despite no ellipticity selection. We note that some $H\alpha$ filaments are present in the imaging of UCDs around NGC 1275.

4.1 Background contamination

A possible source for contamination in our sample of Perseus cluster UCDs is background galaxies. Such objects may appear as round, compact objects with colours and angular sizes similar to UCDs at the distance of Perseus. Therefore, to calculate the likely contamination of such objects in our sample, we need to utilize a deep survey that is free of low-redshift objects which may have their own UCD/GC systems and with similar filters to the data we have used for our UCD search in Perseus.

To estimate the background contamination in our UCD sample, we utilize two fields from the Great Observatories Origins Deep Survey (GOODS) ACS survey, with one field taken from GOODS-North and another field taken from GOODS-South. We use section 33 of the north mosaic, and section 22 of the south mosaic. Version 1 of the imaging is used in our analysis, which is of sufficient depth to allow comparison to our imaging. The survey area covered by each mosaic section is 404×404 arcsec², approximately four times the survey area of a single pointing of ACS. We therefore utilize two mosaic cut-outs to approximate our survey area. The imaging was taken in the *F606W* and *F775W* bands, which can be easily converted to *V* and *I* using Sirianni et al. (2005).

Objects are identified using the same *SEXTRACTOR* code as in our initial object identification. The PSF was then constructed using the *IRAF DAOPHOT* task for each mosaic section. Fitting of all objects with *ISHAPE* was then performed, and the final catalogues cleaned of stars and obvious background galaxies. The sizes, colours and magnitudes of the remaining objects were then examined in Fig. 5.

In general, the colours of UCD-like objects in the GOODS fields are not consistent with those found for UCD candidates in Perseus ($V - I \sim 1$). UCD-sized objects in the comparison fields are typically very blue in colour, with $V - I < 0.5$, and are therefore likely strongly star-forming, high-redshift galaxies. Furthermore, these objects are in general faint, with $I < 23.5$, and the majority of these objects would not be of sufficient S/N to make the UCD candidate list due to the shallower depth of our imaging.

All UCD candidates we identify in our *F555W* and *F814W* band imaging are brighter than $I = 24$, with colours $0.7 < (V - I) <$

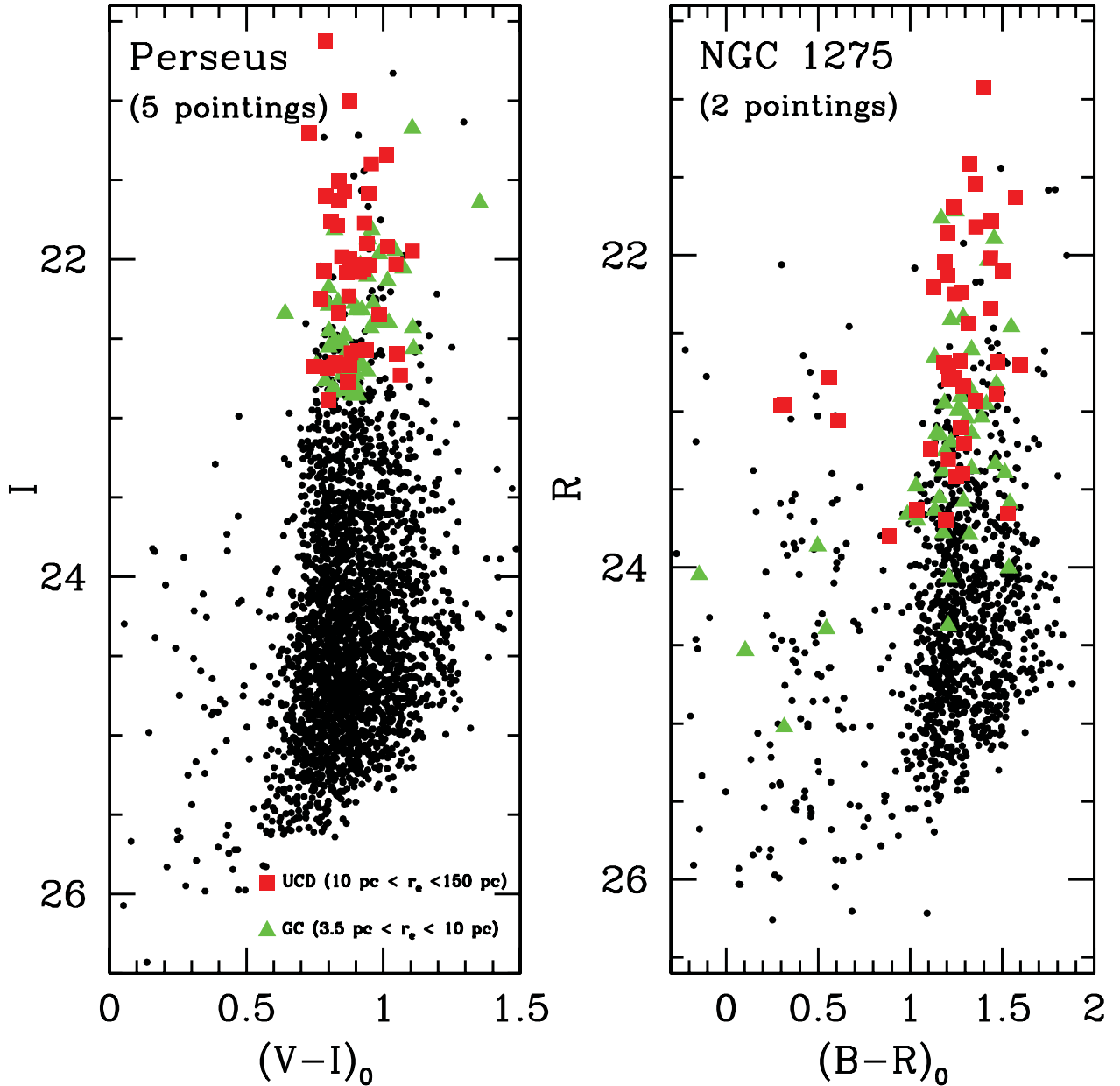


Figure 2. Colour–magnitude diagrams for the compact stellar objects around NGC 1275 (right), and the five pointings covering the rest of the Perseus cluster (left). We have removed stars, background objects and other contaminants from our sample, but otherwise we include all objects with effective radii 1–150 pc. Sequences defined by the compact stellar systems are visible, with a small additional population of blue $(B - R)_0 \sim 0.4$ star clusters seen for NGC 1275. Objects with reliable size measurements ($S/N > 40$ and $r_e < 3.5$ pc) are highlighted, with UCDs denoted by red squares, and GCs by green triangles. All other objects are denoted by black dots, and have insufficient S/N to have accurate sizes determined, else are smaller than 3.5 pc.

1.2. For the GOODS-N imaging, only one object has a colour, size and magnitude that falls within the size–colour–magnitude space occupied by ‘normal’ Perseus UCDs. For the GOODS-S field, two such objects are seen. As a result of this exercise, we consider the likely contamination from background sources in our candidate list to be small (2–3 objects). As we have no redshifts at this stage, all UCDs presented in this paper are candidates, with follow-up spectroscopy essential to establish cluster membership.

For the young, blue UCDs around NGC 1275, the contamination from background objects becomes more of a concern. Another way to establish the likelihood of cluster membership for compact objects is to examine the radial surface density distribution around their host galaxy. We expect the number of compact systems to

fall off with increasing galactocentric distance, before the distribution flattens at large radii to a constant background radius. At large radii the probability of an object being a background contaminant therefore increases.

We investigate the surface density distribution of all star clusters in our sample around NGC 1275 in Fig. 6. The survey region around NGC 1275 is contiguous, with only compact objects in the very inner regions of the galaxy excluded from our search. Therefore we can examine the radial distribution of compact objects in this region of the cluster. The surface density plots for GCs ($r_e < 10$ pc) and UCDs ($10 < r_e < 150$ pc) are both plotted. For GCs, the distribution flattens in the inner regions ($D < 1$ arcmin), where a combination of the fact that we were not able to remove the central galaxy and

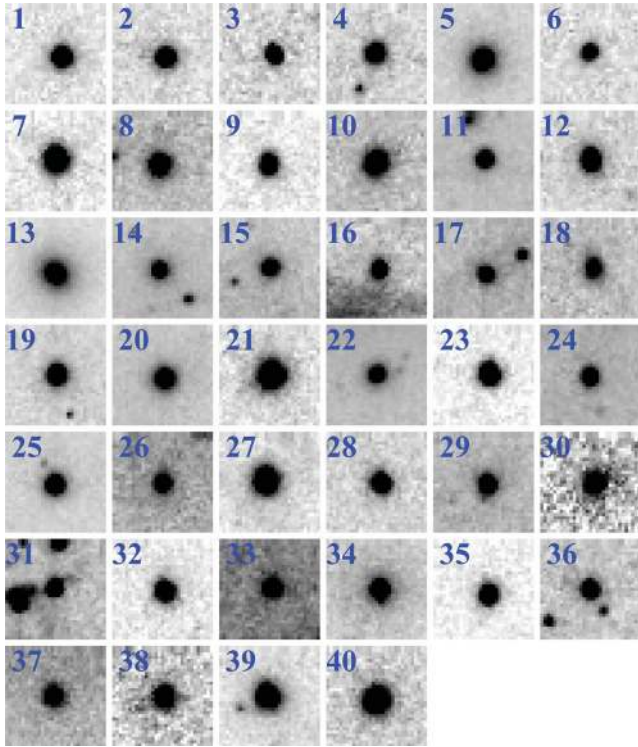


Figure 3. *F625W* band images of 40 candidate UCDs in the vicinity of NGC 1275. The cut-outs measure $2 \times 2 \text{ arcsec}^2$ ($700 \times 700 \text{ pc}^2$ at the distance of Perseus). All objects were selected to have sizes $10 < r_e < 150 \text{ pc}$, though the largest object in our sample has $r_e = 57 \text{ pc}$. The ID numbers in the top left-hand corner of each cut-out are those given in Table 2, which also lists their positions, magnitudes and colours.

tidal effects start to come into account. A power law of slope -1.6 is fit to the GC radial surface density distribution for $D > 1 \text{ arcmin}$.

The radial density distribution also flattens for UCDs, but at distances $D < 1.5 \text{ arcmin}$ (30 kpc). This could imply that UCDs are not commonly formed at these galactocentric distances, else large star clusters are more likely to be tidally truncated at small distances from their host galaxy. However, at larger radii both populations follow the same radially decreasing distribution within the error bars. This suggests UCDs and GCs have a similar parent population. This distribution does not flatten off to our largest galactocentric distance, showing the majority of objects in this study are associated with the host galaxy.

The fact that the radial surface distributions of both GCs and UCDs around NGC 1275 do not flatten off at large radii in this plot, shows that objects in this study are statistically associated with NGC 1275. Therefore given the proximity of the three young, blue UCDs to NGC 1275 ($D = 12.8, 21.0, 23.5 \text{ kpc}$), and the fact that they are located near filaments with ongoing star formation, we consider these likely members of the Perseus cluster associated with NGC 1275.

4.2 UCDs around NGC 1275

To separate UCDs and GCs, we plot the effective radius versus absolute magnitude for all objects with $S/N > 40$ in *F555W* in Fig. 7. All objects with sizes $r_e > 10 \text{ pc}$ are taken to be UCDs. Based on their sizes (Fig. 7), we identify a total of 40 UCD-sized candidates around the cluster-centred galaxy NGC 1275 with sizes

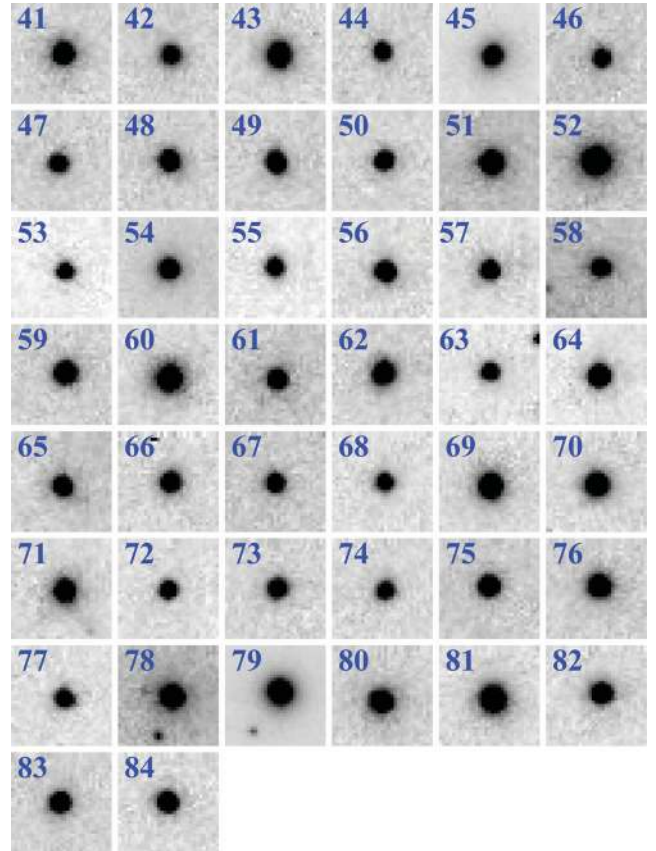


Figure 4. *F814W* images of the remaining 44 UCD candidates in the Perseus cluster core identified from *F555W* and *F814W* imaging. The cut-outs measure $2 \times 2 \text{ arcsec}^2$ ($700 \times 700 \text{ pc}^2$ at the distance of Perseus). The number in the top left-hand corner is the ID number assigned to each UCD in Table 3.

$10 < r_e < 57 \text{ pc}$ and magnitudes between $R = 20.97$ and 23.80 ($R \approx -14$ to ≈ -10.5 , respectively). Following the methodology of Brodie et al. (2011), we have not restricted the luminosity range for UCDs. We have also made no selection by ellipticity or colour, as not to limit our sample to old, passive systems. The properties of these objects are listed in Table 2, with their colours and magnitudes shown in Fig. 8. The UCDs have ellipticity values of b/a between 0.6 and 1, consistent with ellipticities found in previous studies (Madrid et al. 2010), with a mean ratio $b/a = 0.82 \pm 0.11$.

The majority of these UCDs lie on the same colour–magnitude trend followed by the GCs in this region. Furthermore, it can be seen that some UCDs typically follow the ‘blue tilt’ seen for the GC blue subpopulation of NGC 1275, with a smaller number of UCDs lying on the red GC subpopulation.

Unusually, not all of the UCD candidates we identify have colours typically found for UCDs and GCs to date, i.e. they do not all lie on a bright extension of the GC colour–magnitude trend. Three of these objects (UCD17, UCD29 and UCD31) are bluer than typical UCDs, with $(B - R)_0$ colours of 0.28, 0.54 and 0.59, respectively. We refer to these objects as blue UCDs from here onwards. Another object, UCD18, has a colour of $(B - R)_0 = 0.86$, intermediate between a blue star-forming object and a normal UCD. In addition to these UCDs, a number of round objects are embedded in the star-forming filaments that are likely young GCs and UCDs, and can be seen in Fig. 2. However, these regions are too crowded for accurate sizes to be determined for these objects using *ISHAPE*. They lie in the

Table 2. UCDs in the vicinity of NGC 1275 identified from $F435W$ and $F625W$ imaging.

UCD	α (J2000.0)	δ (J2000.0)	R (mag)	$(B - R)_0$ (mag)	$r_{e,F625W}$ (pc)	b/a
UCD1	03:19:37.64	+41:29:43.8	22.81 ± 0.02	1.18 ± 0.05	11.7	0.97
UCD2	03:19:39.79	+41:30:17.2	22.90 ± 0.03	1.44 ± 0.06	26.9	0.73
UCD3	03:19:40.00	+41:28:58.7	23.66 ± 0.04	1.50 ± 0.08	11.2	0.62
UCD4	03:19:40.16	+41:30:33.2	23.12 ± 0.03	1.25 ± 0.06	18.9	0.63
UCD5	03:19:40.72	+41:30:53.4	21.45 ± 0.01	1.29 ± 0.03	24.8	0.91
UCD6	03:19:40.89	+41:29:59.3	23.63 ± 0.03	1.01 ± 0.07	10.4	0.61
UCD7	03:19:41.03	+41:32:11.1	22.04 ± 0.02	1.41 ± 0.04	12.5	0.82
UCD8	03:19:41.17	+41:30:49.2	22.70 ± 0.02	1.44 ± 0.05	13.9	0.97
UCD9	03:19:41.60	+41:32:07.9	22.85 ± 0.02	1.26 ± 0.05	14.4	0.60
UCD10	03:19:41.66	+41:30:22.3	22.46 ± 0.02	1.29 ± 0.04	17.6	0.78
UCD11	03:19:44.36	+41:31:04.3	22.27 ± 0.02	1.21 ± 0.04	13.1	0.93
UCD12	03:19:44.64	+41:28:59.6	22.70 ± 0.02	1.16 ± 0.05	20.8	0.75
UCD13	03:19:45.13	+41:32:06.0	20.97 ± 0.01	1.37 ± 0.03	57.0	0.96
UCD14	03:19:45.56	+41:30:43.8	22.07 ± 0.02	1.16 ± 0.04	13.1	0.99
UCD15	03:19:45.95	+41:30:33.3	22.69 ± 0.02	1.24 ± 0.05	13.6	0.88
UCD16	03:19:48.06	+41:31:52.0	22.26 ± 0.02	1.25 ± 0.06	15.2	0.75
UCD17	03:19:48.56	+41:31:17.8	22.97 ± 0.03	0.28 ± 0.04	18.4	0.84
UCD18	03:19:49.11	+41:29:42.9	23.80 ± 0.04	0.86 ± 0.07	33.0	0.80
UCD19	03:19:49.96	+41:31:21.6	21.88 ± 0.02	1.17 ± 0.03	13.1	0.85
UCD20	03:19:49.96	+41:30:10.3	21.72 ± 0.01	1.21 ± 0.03	15.7	0.92
UCD21	03:19:50.05	+41:32:08.9	22.23 ± 0.02	1.10 ± 0.04	31.2	0.94
UCD22	03:19:50.14	+41:30:39.9	21.81 ± 0.02	1.41 ± 0.04	13.1	0.80
UCD23	03:19:50.15	+41:29:14.3	22.36 ± 0.02	1.41 ± 0.05	11.5	0.75
UCD24	03:19:51.32	+41:30:44.7	22.73 ± 0.02	1.18 ± 0.05	19.2	0.85
UCD25	03:19:51.43	+41:30:17.3	21.66 ± 0.01	1.54 ± 0.03	11.5	0.83
UCD26	03:19:51.80	+41:31:33.9	23.32 ± 0.03	1.18 ± 0.06	13.9	0.76
UCD27	03:19:51.80	+41:29:44.4	21.58 ± 0.01	1.32 ± 0.03	16.3	0.84
UCD28	03:19:52.27	+41:29:42.3	22.95 ± 0.03	1.32 ± 0.05	11.7	0.74
UCD29	03:19:52.79	+41:30:16.0	22.80 ± 0.02	0.54 ± 0.04	22.4	0.78
UCD30	03:19:52.83	+41:29:16.3	23.70 ± 0.04	1.17 ± 0.08	14.9	0.86
UCD31	03:19:52.96	+41:30:04.6	23.04 ± 0.03	0.55 ± 0.05	10.7	0.73
UCD32	03:19:53.01	+41:32:25.8	23.25 ± 0.03	1.08 ± 0.06	29.8	0.64
UCD33	03:19:53.10	+41:30:15.9	23.21 ± 0.03	1.27 ± 0.06	10.4	0.83
UCD34	03:19:53.53	+41:30:20.4	22.15 ± 0.02	1.17 ± 0.04	16.8	1.00
UCD35	03:19:54.08	+41:29:26.1	22.80 ± 0.02	1.21 ± 0.05	18.6	0.67
UCD36	03:19:54.98	+41:30:22.7	22.72 ± 0.02	1.56 ± 0.06	39.7	0.74
UCD37	03:19:57.19	+41:31:11.1	23.43 ± 0.03	1.22 ± 0.07	25.3	0.97
UCD38	03:19:57.23	+41:29:19.2	23.40 ± 0.03	1.26 ± 0.07	11.5	0.80
UCD39	03:19:58.08	+41:32:39.6	21.85 ± 0.02	1.33 ± 0.04	22.1	0.89
UCD40	03:19:58.74	+41:29:55.1	22.12 ± 0.02	1.47 ± 0.04	13.9	0.78

magnitude range $-8.26 < M_R < -12.25$, and their colours are in the range $-0.2 < (B - R)_0 < 0.71$, again consistent with a population that has recently ceased star formation.

Similar to Canning et al. (2010), we examine the ages of the NGC 1275 UCDs by comparing their colours to Bruzual & Charlot (2003) models for the colour evolution of a simple stellar population since the last burst of star formation (Fig. 9). The colours of the normal UCDs, i.e. those with $(B - R)_0 > 1.0$ are consistent with objects that have not undergone star formation in the past Gyr. However, the UCD candidates with colours bluer than this are likely much younger objects, with the blue object at $(B - R)_0 = 0.28$ having a stellar age ~ 100 Myr. This is consistent with the results of Canning et al. (2010) for blue star clusters in this region.

Several of the red UCDs in the vicinity of NGC 1275 are also located in the regions of the filaments. Red UCDs at the projected distance of these filaments must have survived at least 1 Gyr since their formation without being tidally disrupted or destroyed by their host galaxy. Fig. 10 shows examples of blue and red UCDs residing

in or near filaments, along with clumpy regions of star formation that might be responsible for the formation of at least some UCDs and GCs (see the discussion in Section 6).

We consider the fact that we may be missing some young, blue star clusters due to patches of dust visible in NGC 1275, which would cause internal reddening. As a result of this dust, a possible source of contamination in our ‘normal’ UCDs could arise from bright, young massive star clusters that have been reddened by this dust. We consider this scenario unlikely as we see no bright blue star clusters that are round in shape in regions far away enough from the galaxy core that such internal reddening is unlikely to occur. It can be seen from Fig. 2 and Table 2 that the youngest blue UCD around NGC 1275 has $(B - R)_0 \sim 0.3$. For a blue star cluster to be sufficiently reddened to move it on to the blue or red sub-populations requires a colour shift ~ 1 mag. Such an object would also be dimmed by a similar amount. Assuming a similar correction to the Galactic reddening correction applied in the direction of Perseus ($A_B = 0.435$, $A_R = 0.703$), there are no blue objects around

Table 3. UCDs identified from our *F555W* and *F814W* band imaging covering five fields of the Perseus core.

UCD	α (J2000.0)	δ (J2000.0)	I (mag)	$(V - I)_0$ (mag)	$r_{e,F814W}$ (pc)	b/a
UCD41	03:19:00.38	+41:31:29.6	21.80 ± 0.02	0.94 ± 0.04	19.2	0.98
UCD42	03:19:01.72	+41:33:25.6	22.61 ± 0.03	1.06 ± 0.06	22.9	0.90
UCD43	03:19:03.03	+41:30:54.9	21.81 ± 0.02	0.84 ± 0.04	33.3	0.87
UCD44	03:19:04.69	+41:32:03.8	22.69 ± 0.03	0.83 ± 0.06	10.4	0.61
UCD45	03:19:08.07	+41:29:16.7	20.67 ± 0.01	0.80 ± 0.03	33.8	0.85
UCD46	03:19:09.73	+41:28:56.9	22.70 ± 0.03	0.81 ± 0.06	11.7	0.81
UCD47	03:19:11.26	+41:30:59.4	22.68 ± 0.03	0.88 ± 0.06	14.7	0.94
UCD48	03:19:13.29	+41:32:47.3	22.10 ± 0.03	0.88 ± 0.05	14.1	0.82
UCD49	03:19:13.33	+41:31:55.1	22.09 ± 0.03	0.79 ± 0.05	16.0	0.52
UCD50	03:19:13.70	+41:34:22.8	22.36 ± 0.03	0.99 ± 0.06	11.2	0.81
UCD51	03:19:17.07	+41:29:24.0	21.37 ± 0.02	1.02 ± 0.04	14.4	0.91
UCD52	03:19:17.24	+41:32:32.4	21.04 ± 0.02	0.88 ± 0.03	22.6	0.97
UCD53	03:19:20.02	+41:31:38.6	22.79 ± 0.03	0.88 ± 0.06	15.7	0.80
UCD54	03:19:20.04	+41:28:51.9	21.23 ± 0.02	0.74 ± 0.03	18.1	0.96
UCD55	03:19:25.21	+41:31:37.4	22.61 ± 0.03	1.06 ± 0.06	18.4	0.98
UCD56	03:19:25.56	+41:30:49.6	22.02 ± 0.02	0.88 ± 0.05	11.2	0.89
UCD57	03:19:26.15	+41:34:29.0	22.10 ± 0.03	0.89 ± 0.05	13.3	0.85
UCD58	03:19:27.57	+41:32:43.9	22.25 ± 0.03	0.88 ± 0.05	13.3	0.53
UCD59	03:19:28.14	+41:28:55.9	21.94 ± 0.02	1.02 ± 0.05	18.6	0.90
UCD60	03:19:28.30	+41:34:30.0	21.43 ± 0.02	0.96 ± 0.04	49.0	0.95
UCD61	03:19:28.37	+41:29:11.3	22.36 ± 0.03	0.85 ± 0.05	24.8	0.99
UCD62	03:19:29.36	+41:32:54.5	21.97 ± 0.02	1.11 ± 0.05	20.0	0.84
UCD63	03:19:31.41	+41:30:21.9	22.59 ± 0.03	0.91 ± 0.06	10.9	0.82
UCD64	03:19:32.83	+41:34:33.9	21.60 ± 0.02	0.87 ± 0.04	13.3	0.97
UCD65	03:19:33.31	+41:34:34.3	22.05 ± 0.02	1.05 ± 0.05	13.6	0.64
UCD66	03:19:34.88	+41:32:28.7	22.27 ± 0.03	0.78 ± 0.05	15.7	0.88
UCD67	03:19:37.95	+41:32:04.8	22.67 ± 0.03	0.83 ± 0.06	14.7	1.00
UCD68	03:19:38.34	+41:26:43.2	22.74 ± 0.03	1.07 ± 0.07	17.3	0.67
UCD69	03:19:38.86	+41:27:42.0	21.54 ± 0.02	0.85 ± 0.04	22.1	0.89
UCD70	03:19:40.47	+41:28:09.3	21.78 ± 0.02	0.82 ± 0.04	20.0	0.98
UCD71	03:19:40.88	+41:28:03.7	21.93 ± 0.02	0.95 ± 0.05	26.1	0.80
UCD72	03:19:42.19	+41:33:59.5	22.69 ± 0.03	0.76 ± 0.06	10.1	0.99
UCD73	03:19:42.26	+41:28:42.5	22.60 ± 0.03	0.89 ± 0.06	21.8	0.92
UCD74	03:19:42.46	+41:27:35.5	22.90 ± 0.04	0.81 ± 0.07	21.0	0.71
UCD75	03:19:43.11	+41:29:05.6	22.10 ± 0.03	0.92 ± 0.05	12.3	0.89
UCD76	03:19:45.82	+41:28:45.8	22.01 ± 0.02	0.86 ± 0.04	24.5	0.99
UCD77	03:19:46.10	+41:26:58.5	22.59 ± 0.03	0.94 ± 0.06	11.7	0.98
UCD78	03:19:47.59	+41:29:25.0	21.63 ± 0.02	0.80 ± 0.04	23.4	0.94
UCD79	03:19:49.63	+41:28:35.4	19.91 ± 0.01	1.10 ± 0.02	27.4	0.94
UCD80	03:19:50.61	+41:27:41.8	21.61 ± 0.02	0.96 ± 0.04	16.0	0.95
UCD81	03:19:53.52	+41:28:04.0	21.65 ± 0.02	0.85 ± 0.04	46.1	0.88
UCD82	03:19:53.54	+41:28:12.7	22.06 ± 0.02	0.96 ± 0.05	17.0	0.92
UCD83	03:19:53.80	+41:28:57.6	22.08 ± 0.03	0.94 ± 0.05	11.2	0.74
UCD84	03:19:55.47	+41:27:54.0	22.05 ± 0.02	0.94 ± 0.05	10.9	0.79

NGC 1275 sufficiently bright to masquerade as red UCDs reddened by their host galaxy. Similarly, even with a reddening vector $A_V = 1$, there are no objects today to be reddened into the colour range exhibited by ‘normal’ UCDs (see Fig. 8).

4.3 UCDs in the rest of the cluster

We also identify a total of 44 candidate UCDs in our *F555W* and *F814W* imaging, which includes the bright elliptical NGC 1272. As for the NGC 1275 region, we select UCD candidates to have sizes $10 < r_e < 150$ pc, and we make no selection based on either luminosity or colour. These objects have sizes $10 < r_e < 49$ pc, magnitudes brighter than $M_V = -11$ and colours $0.7 < (V - I) < 1.1$. Their mean ellipticity b/a is 0.87. The sizes of these objects

are shown in Fig. 11, with their colours and magnitudes included in Fig. 12. Also included on this plot are the colours of dEs in the cluster core identified in de Rijcke et al. (2009) and Penny et al. (2009), along with GCs identified in this work. The colours and magnitudes of Perseus dE nuclei are also shown to investigate any similarities between UCDs and dE nuclei. To compare the colours of the UCDs and dEs, we perform a least-squares fit to the dE population for all dEs brighter than $M_I = -13.5$. dEs fainter than this are excluded due to a small sample size at the faint end. The UCDs follow the extrapolated colour–magnitude relation (CMR) of the dEs down to $M_I = -11$.

The CMR for dEs is interpreted as a mass–metallicity relation, such that brighter dwarfs are more metal rich and therefore have redder colours. In Penny & Conselice (2008), we found that the

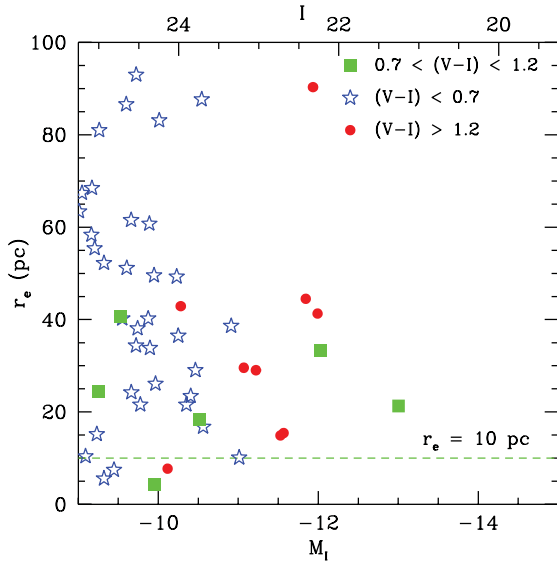


Figure 5. The size–magnitude relation for compact objects identified from GOODS ACS imaging, used to estimate the likely contamination of our sample from background galaxies. The squares represent high-redshift objects that would be identified as UCDs under our selection criteria and fall in the colour range occupied by ‘normal’ Perseus UCD candidates ($0.7 < V - I < 1.2$). The stars are objects with colours bluer than Perseus UCDs, and red dots are those redder than typical UCD colours.

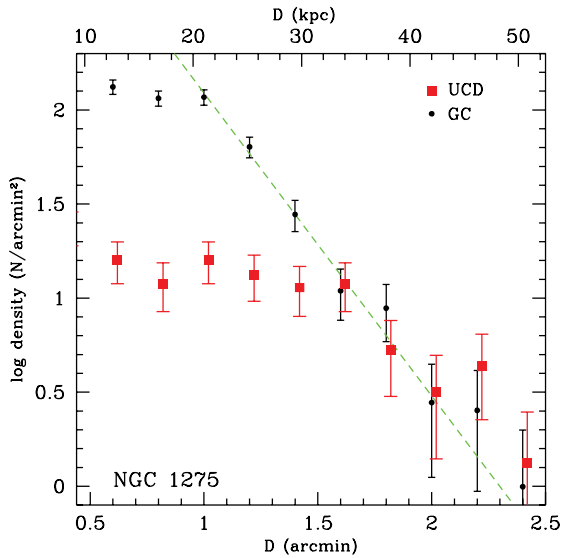


Figure 6. Radial surface density of compact objects around NGC 1275. The red squares are the UCDs, with the dots representing GCs. The UCD radial surface densities are arbitrarily shifted to allow comparison between the radial surface density distributions of the UCDs and GCs. A small offset of $+0.02$ arcmin in distance is applied to UCD data set to allow easier comparison of the two populations. The error bars are Poissonian errors on the number counts for each radial bin. The green dashed line is a power-law fit to the data of slope -1.6 . The density for both UCDs and GCs do not flatten out at larger radii, showing that all objects we identify here are statistically associated with NGC 1275, and we have not reached the background level.

spectra of cluster dEs are consistent with ages >2 Gyr, and therefore have little age information left in their colours. The more luminous galaxies have deeper potentials and therefore retain their metal content more effectively. As a result, more massive dwarfs can

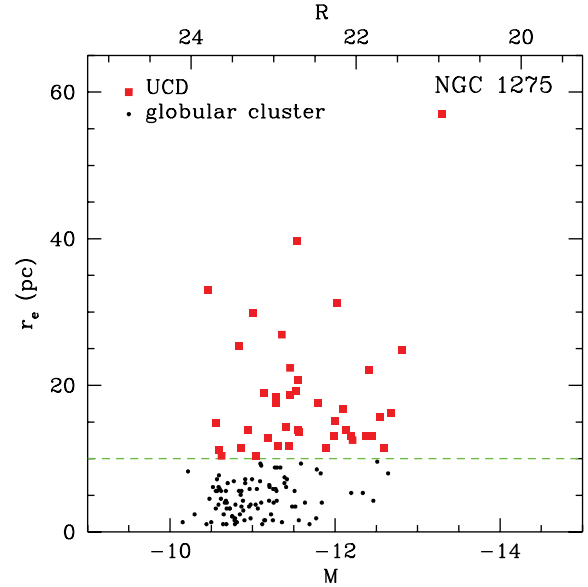


Figure 7. Size–magnitude diagram for objects around NGC 1275. The dashed line corresponds to an effective radius of 10 pc, which is taken to be the size separating the GC and UCD populations. All objects have $S/N > 40$. The red points are UCDs, and the black points are GCs.

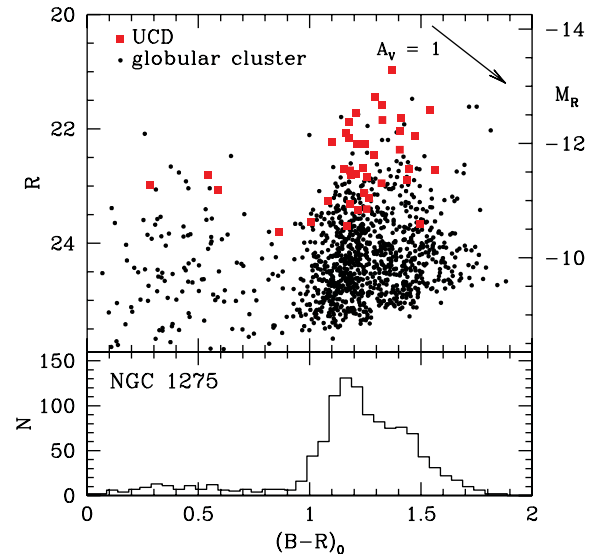


Figure 8. The colour distribution of compact stellar systems around NGC 1275. The colours of the GC system appear bimodal, with blue and red subpopulations. The arrow shows the direction and magnitude of the reddening vector. UCDs around NGC 1275 are marked by red boxes. Most NGC 1275 UCDs lie on the bright end of the blue GC subpopulation, with fewer red subpopulation UCDs. A small number of very blue UCDs are seen.

self-enrich to higher levels than less massive ones. UCDs continue this mass–metallicity relation to fainter magnitudes. dE nuclei and UCDs also occupy the same region of colour–magnitude space, as has been noted by other authors (e.g. Brodie et al. 2011).

4.4 The UCD size–magnitude relation

We compare the sizes and colours of the UCDs we have identified to those found for UCDs in other groups and clusters, along with the

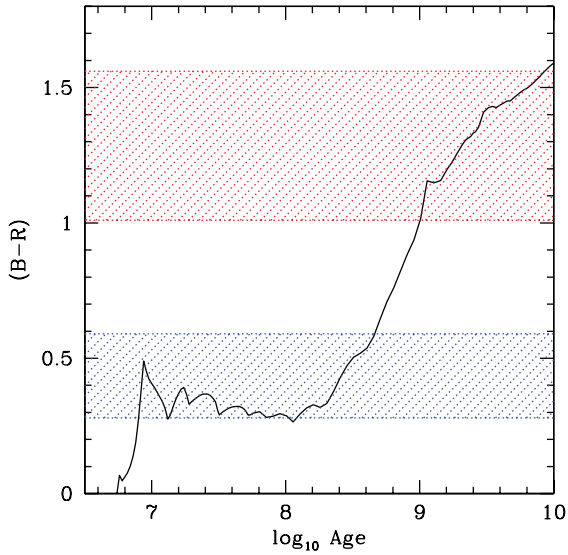


Figure 9. Colour–age predictions for the UCDs around NGC 1275. The colours of the NGC 1275 UCDs are compared to the Bruzual & Charlot (2003) models for how colour evolves with age, using a Salpeter initial mass function. The model is shown as a solid line, corresponding to a metallicity of $0.02 (Z_{\odot})$. It can be seen that the very blue UCDs have ages consistent with a recent cessation of star formation, having young ages of 10–100 Myr. The UCDs with ‘typical’ colours are consistent with no recent star formation, and ages > 1 Gyr.

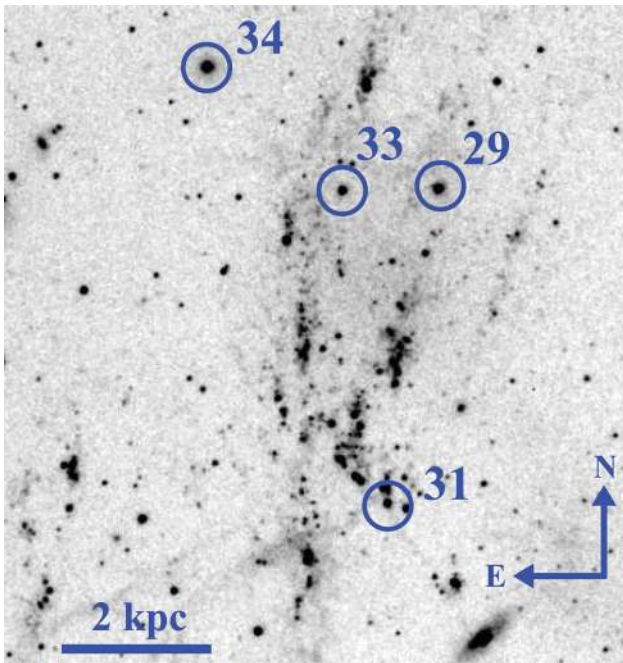


Figure 10. R -band image showing a star-forming filament near NGC 1275. The background gradient due to NGC 1275 has been removed. UCDs in this region are circled, with their identification numbers from Table 2 also shown. A solid bar of length 2 kpc is provided for scale. Embedded in the filaments are numerous massive, young, blue star clusters. UCDs 29 and 31 are bluer than typical UCDs with $(B - R)_0 < 0.6$.

sizes found for dEs and compact galaxies taken from the literature in Fig. 13. Much of our literature sample matches that of Misgeld & Hilker (2011). We add to this sample our own data for the sizes of the Perseus dEs (de Rijcke et al. 2009), and include the UCD sample

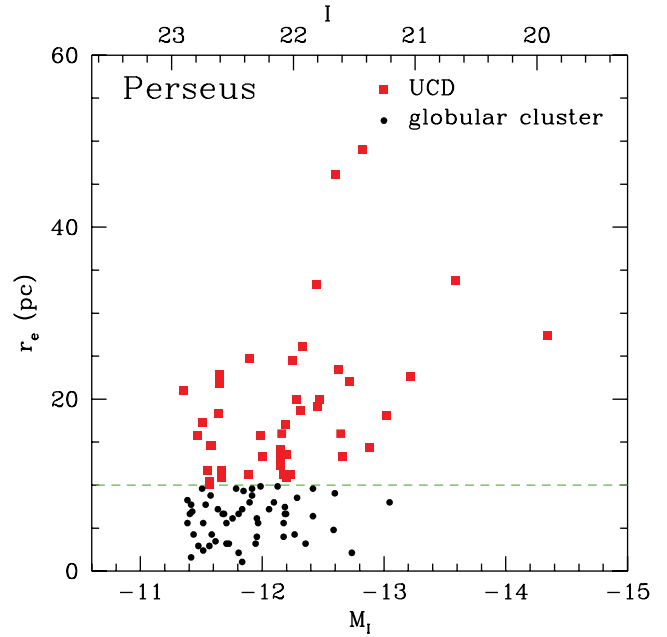


Figure 11. Size–magnitude diagram for compact objects identified in the regions covered by our $F555W$ and $F814W$ band HST ACS imaging. The symbols and lines have the same meaning as for Fig. 7.

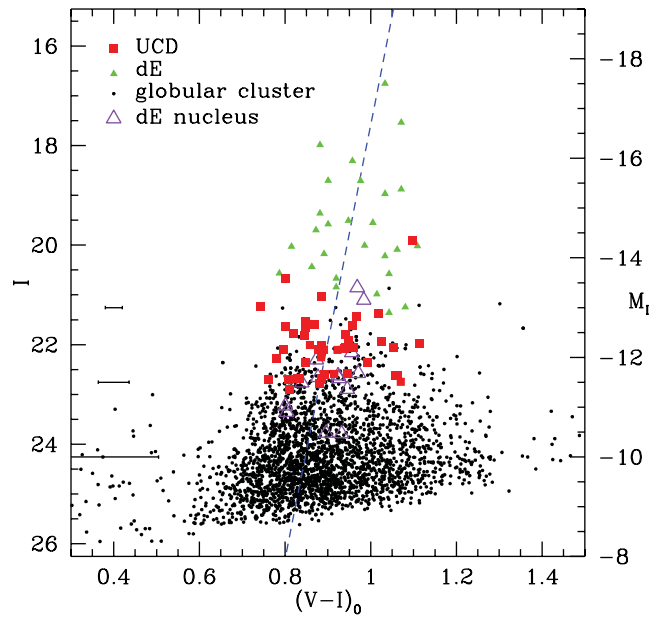


Figure 12. CMR for all UCDs identified from the $F555W$ and $F814W$ band imaging (red squares). GCs ($r_e < 10$ pc) are shown as black dots. The Perseus dE sample identified in Penny et al. (2009) and de Rijcke et al. (2009) is also included for comparison as green triangles. Typical error bars at various magnitudes for the colours of the UCDs and GCs are given. The blue dashed line is a fit to the CMR for dEs brighter than $M_1 = -13.5$. The UCDs are consistent with the dE CMR extrapolated to lower magnitudes. dE nuclei are also shown as blue triangles. This plot is best viewed in colour in the online version of the journal.

from Brodie et al. (2011). Also included on this plot are the four UCDs identified from R -band imaging in the vicinity of NGC 1275 with sizes > 30 pc. Their B -band magnitudes are converted to V using the conversion of $B - V = 0.96$ from Fukugita, Shimasaku & Ichikawa (1995) for an elliptical galaxy.

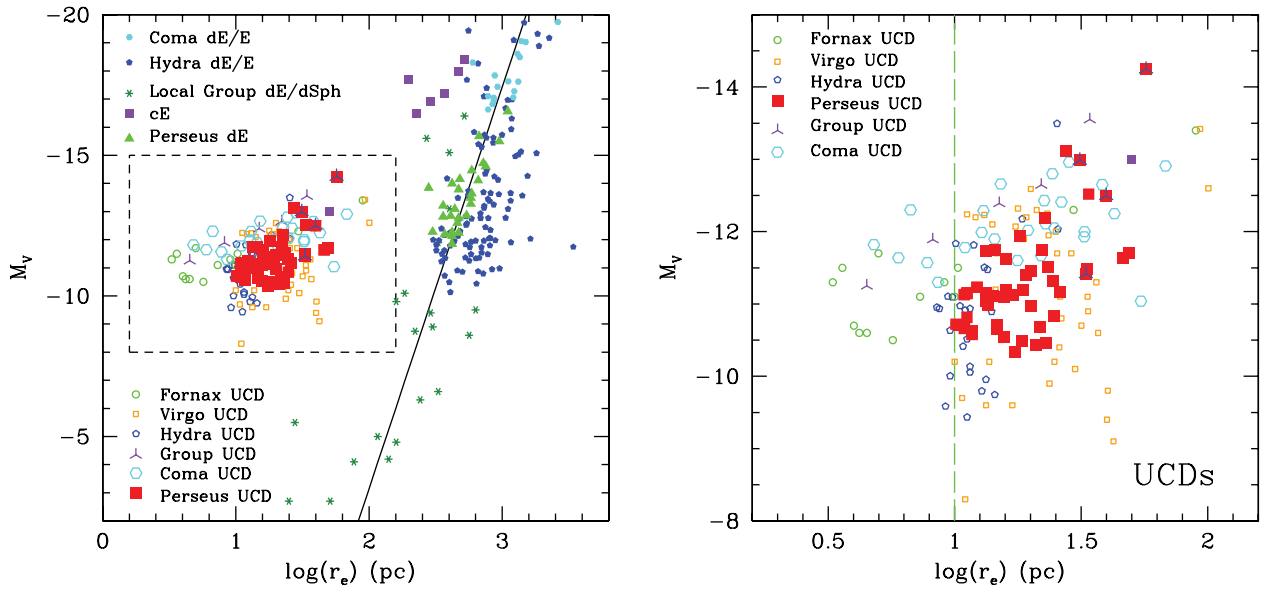


Figure 13. Absolute luminosity versus effective radius for UCDs identified in our Perseus $F555W$ and $F814W$ band imaging. The Perseus UCDs are represented by red squares. The red squares containing blue crosses are large UCDs ($r_e > 30$ pc) identified from the $F435W$ and $F625W$ imaging around NGC 1275 that have had their B -band luminosities converted to V band using the conversion of Fukugita et al. (1995) for an elliptical galaxy. The green dashed line in the right-hand plot corresponds to $r_e = 10$ pc. Additional data from the literature as described in the main text of the paper are also included. The left-hand plot shows the sizes of UCDs along with cEs and dEs/dSphs, with the region of the plot occupied by UCDs enclosed by the dashed box. The right-hand plot showing UCDs only (the region surrounded by a dashed box in the left-hand plot). The solid line in the left-hand plot is a linear fit to the size–luminosity relation for dEs is from de Rijcke et al. (2009). This plot is best viewed in colour on the online version of the paper.

The data we use are as follows: Brodie et al. (2011) and Evstigneeva et al. (2008) for Virgo UCDs; Mieske et al. (2008) for Fornax UCDs; Chiboucas et al. (2011) for Coma UCDs; Misgeld & Hilker (2011) for Hydra compact objects; Misgeld, Mieske & Hilker (2008) for Hydra dEs; Norris & Kannappan (2011) for UCDs in nearby galaxy groups (around NGC 3923, NGC 4546 and the Sombrero Galaxy); Graham & Guzmán (2003) for the Coma dEs; Martin, de Jong & Rix (2008) for Local Group dSphs; Gilmore et al. (2007) for the sizes of Local Group objects, with Grebel, Gallagher & Harbeck (2003) for the photometry of these objects. We also utilize sizes from de Rijcke et al. (2009) for the Perseus dEs. All the UCD data sets included in Fig. 13 have spectroscopically confirmed cluster membership.

We convert the B -band colours of Graham & Guzmán (2003) to V band using the $B - V$ CMR constructed as used in de Rijcke et al. (2009). This relation changes from $B - V \sim 0.7$ at $M_B = -8$ to $B - V \sim 0.8$ at $M_B = -22$. We therefore apply a constant mean colour correction $\langle B - V \rangle = 0.8$ for this data, as most of it is at the bright end of the CMR. We perform a similar conversion for the UCD sample of Madrid et al. (2010).

The sizes and magnitudes for the UCDs we identify in this study agree well with those found in other regions of the Universe, which all have spectroscopically confirmed group/cluster membership. We find no low luminosity, extended GCs/UCDs that might fill in the gap between the sequence of galaxies and compact star clusters, i.e. objects with $r_e \sim 100$ pc and $M_V < -15$. Objects with more extended effective radii and faint magnitudes would have very low surface brightness, making them difficult to detect in existing surveys of higher redshift ($D > 30$ Mpc) clusters such as Perseus. In addition, the gap of objects with sizes $80 < r_e < 150$ pc remains on the sequence formed by cEs and UCDs.

4.5 The distribution of UCDs in the Perseus cluster

The locations of all UCDs in the Perseus cluster covered in our imaging are shown in Fig. 14. It can be seen that UCDs are preferentially

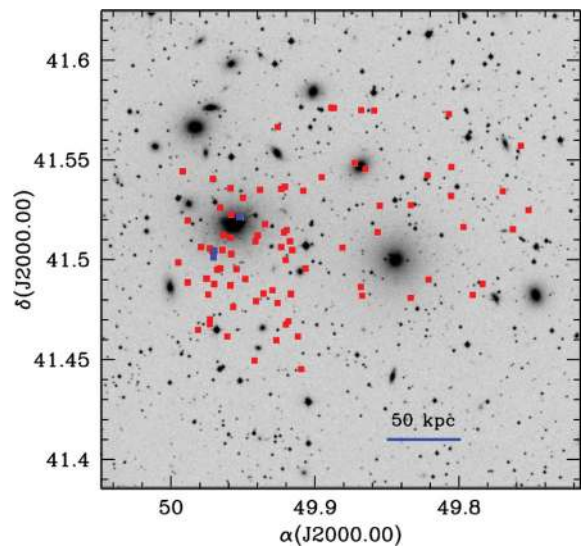


Figure 14. The positions of all compact stellar systems in the Perseus cluster with sizes $10 < r_e < 150$ pc that make our final catalogue of UCDs. The red squares are UCDs with ‘typical’ colours, and the blue boxes are UCDs with very blue colours consistent with a young stellar population. The solid bar is 50 kpc in size. UCD candidates are predominantly found in the very centre of the cluster around NGC 1275. The imaging is not continuous, so further UCDs likely exist in the cluster core.

found in the highest density regions of the cluster. In particular, the region of the cluster around NGC 1275 appears to have a very large population of UCDs. This large population implies the formation of UCDs in Perseus may be linked to NGC 1275, or that UCDs lie in the deepest part of the Perseus potential well. Thus massive star clusters may be forming in the filaments surrounding the galaxy, as suggested by the close projection of NGC 1275 UCDs and the filaments. Alternatively, these objects could be formed via the tidal stripping of nucleated dEs in the very densest regions of the cluster. Formation scenarios for the Perseus UCD population are discussed further in Section 6.

5 COMPARING THE PERSEUS UCD AND GC POPULATIONS

UCDs have been hypothesized to be an extension of the GC population to larger sizes and brighter magnitudes. If they originate from the same population, then GCs and UCDs might be expected to share similar properties e.g. exhibiting similar colour–distance, radial surface density and colour–magnitude trends. To search for similarities between the two populations, we therefore compare the UCDs we have identified to the Perseus GC system.

The cores of rich clusters contain some of the most massive galaxies in the Universe, which have large GC systems. Such GC systems have bimodal distributions, with blue and red subpopulations (e.g. Fig. 15). The blue subpopulation may also reveal a blue tilt, i.e. redder colours at brighter magnitudes. This ‘blue tilt’ is likely a mass–metallicity relation, with the least massive GCs being the most metal poor. It is thought that more massive GCs on this sequence are able to self-enrich to a small extent, thus increasing their metallicity and resulting in the observed tilt (Strader & Smith 2008). The red subpopulation typically exhibits no such tilt. We investigate if these subpopulations can be identified in Perseus and if UCDs follow these colour trends.

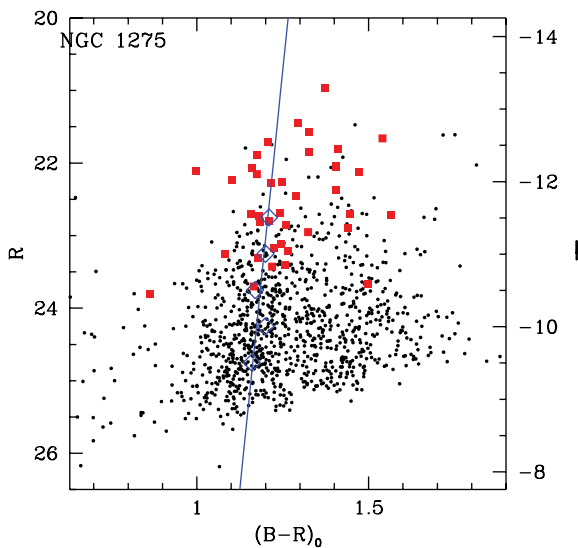


Figure 15. The colour–magnitude diagram for GCs within a projected distance of 50 kpc from NGC 1275. The blue line is a weighted least-squares fit to the blue GC subpopulations. The large open diamonds represent the mean colours of the blue subpopulation as determined using `RMIX`. A significant blue tilt is seen. The fits to the red subpopulation is not included as we do not find a statistically significant red tilt. UCDs in this region are plotted as red squares, and the majority can be seen to lie on the blue and red GC subpopulations.

We define GCs to be all objects in our cleaned catalogues with sizes $1 < r_e < 10$ pc and $S/N > 5$. The lower size limit ensures that stars are not included in our GC sample, with the upper limit of 10 pc to separate of UCDs and GCs. These GCs are drawn from the same visually cleaned catalogues as our UCD sample. To ensure we are sampling GCs rather than background objects, we limit our GC sample to those around massive galaxies where the probability of identifying GCs rather than compact background galaxies is higher. Perseus contains two massive galaxies in its core for which we have (reasonably) complete coverage: NGC 1275 and NGC 1272, therefore, we examine the GC systems of these two massive galaxies.

5.1 The globular cluster system of NGC 1275

The initial colour–magnitude diagram prior to cleaning for all objects detected in the field of NGC 1275 reveals two distinct loci, with a sequence of blue objects not seen in other regions of the cluster. The latter are associated with star-forming regions in the filaments of NGC 1275. This has been observed by several authors to date e.g. Canning et al. (2010). After manual cleaning of clumpy objects in this field, the blue objects mostly disappeared. The remaining objects exhibit typical GC colours ($0.9 < (B - R)_0 < 1.7$).

The remaining objects do not have a simple colour distribution. It can be seen from Fig. 8 that the GC system of NGC 1275 appears to contain red and blue subpopulations. To investigate these subpopulations, we examine the colour distribution for GCs around the galaxy.

We separate the GC population of NGC 1275 into its blue and red subpopulations to determine the blue and red tilts for this galaxy. The GCs are first binned by magnitude into bins of width 0.5 mag. The blue and red peaks of each magnitude bin are then determined using `RMIX`, a package in the programming language `R`, using two Gaussian distributions with fixed σ . We then perform a fit to the colour peaks of the magnitude bins. The very brightest compact objects with $R > 22$ are excluded from this fit due to the small number of objects in this magnitude bin.

The fit to the blue GC subpopulation is found to be

$$(B - R)_0 = (-0.022 \pm 0.008)R + (1.70 \pm 0.196). \quad (1)$$

The fit to the GC red subpopulation:

$$(B - R)_0 = (0.015 \pm 0.011)R + (1.10 \pm 0.264). \quad (2)$$

The result of the fit to the blue subpopulation is included in Fig. 15. A blue tilt is seen for the blue subpopulation, such that fainter objects are bluer than brighter ones. Within the errors, the fit to the red subpopulation has zero slope, suggesting no mass–metallicity relation for these objects.

We also include the UCDs in Fig. 15. The UCDs occupy the bright end of the GC colour–magnitude trend, and lie on the blue and red subpopulations traced by the galaxy’s GC system. These colour–magnitude trends hint that Perseus UCDs might be simple massive GCs.

5.1.1 Radial colour trends in the NGC 1275 GC system

We examine the radial trend in the colour of the NGC 1275 GC system in Fig. 16. First, the projected distances of each GC from NGC 1275 is calculated, and a plot of colour versus projected distance from NGC 1275 is made (Fig. 16). The relations between colour and projected distance for the two subpopulations are fit separately. The GC subpopulations are binned by galactocentric distance, with bins of 5 kpc, and the red and blue means of these

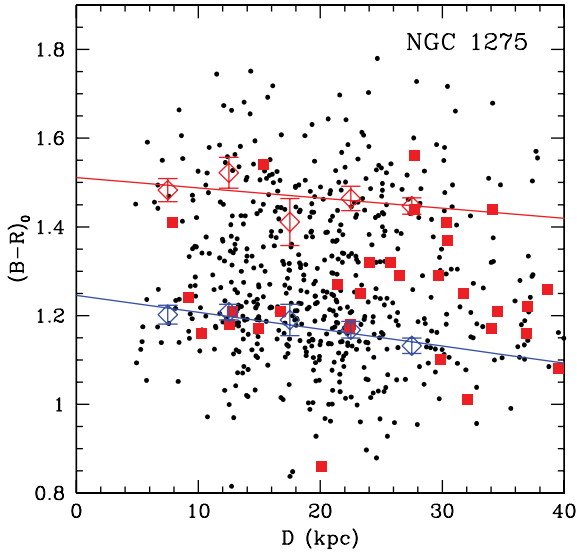


Figure 16. $(B - R)_0$ GC colour versus projected distance from NGC 1275. Blue objects with colours $(B - R)_0 < 0.8$ (i.e. star forming) are excluded from this plot for clarity. The data are binned by galactocentric distance, and the mean colours of the blue and red subpopulations are determined using the R package `RMIX`. The solid lines are linear fits to the binned data. Clear radial trends in colour are seen, with both the blue and red subpopulations becoming bluer with increasing distance from the galaxy centre, suggesting a radial metallicity gradient. The UCDs are included as red squares, with a fraction of these objects following the GC colour–distance relationships.

bins are then found using the same method as for the blue and red tilt fitting. The peaks of each of the radial distance bins are then fitted with a weighted least-squares fit, with each point weighted by $1/\sigma^2$. Objects at a small projected distance from NGC 1275 are excluded from this fit due to the small number of GCs identified in this region.

The radial colour trend in the blue subpopulation is

$$(B - R)_0 = (-0.0038 \pm 0.0012)D + (1.25 \pm 0.024), \quad (3)$$

and for the red subpopulation:

$$(B - R)_0 = (-0.0023 \pm 0.0015)D + (1.51 \pm 0.032), \quad (4)$$

where D is the projected distance from NGC 1275. Within the errors, there is no significant difference in the colour gradients of the two subpopulations as has been found in previous studies (Forbes et al. 2011).

These radial colour trends are likely due to metallicity gradients. The GCs are expected to trace the metallicity gradient of their host halo, as GCs typically host old stellar populations.

The colours and projected distances of the UCDs from NGC 1275 are also included as red squares in Fig. 16. Approximately half of the UCDs follow the colour–distance relation traced by the blue and red GC subpopulations. However, many UCDs at $D > 25$ kpc have colours intermediate between the two GC subpopulations with $(B - R)_0 \sim 1.3$. A least-squares fit to the UCD colour–distance relation for all UCDs redder than $(B - R)_0 = 0.8$ has a slope of 0.0012 ± 0.019 , consistent with zero. Thus we find no radial colour trend in the UCD population around NGC 1275.

5.2 The globular cluster system of NGC 1272

The giant elliptical NGC 1272, located at $\alpha = 03:19:21.3$, $\delta = +41:29:26$ with $M_B = -22.45$ (de Vaucouleurs et al. 1991), is

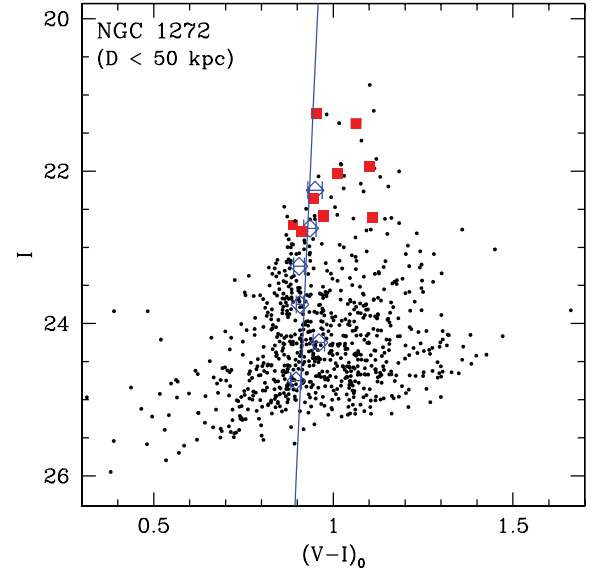


Figure 17. The $(V - I)_0$ CMD for the GC and UCD populations of the second brightest cluster galaxy NGC 1272, out to a distance of 50 kpc. At brighter magnitudes, two colour sequences are seen, corresponding to the red and blue GC subpopulations. The solid line is a weighted least-squares fit to the blue GC subpopulation as determined via Gaussian fitting using `RMIX`. As for NGC 1275, a blue tilt in the GC population is seen. No statistically significant red tilt was found.

the second brightest galaxy in the Perseus cluster. This galaxy is a normal elliptical, and unlike NGC 1275, is relatively easy to fit and remove from our imaging using `IRAF ELLIPSE`. This allows for the identification of compact stellar systems to smaller galactocentric distances.

We fit the blue and red GC subpopulations using the same method as for NGC 1275, with the resulting fit to the blue tilt shown in the colour–magnitude diagram for NGC 1272 GCs (Fig. 17).

The fit to the blue GC subpopulation is

$$(V - I)_0 = (-0.098 \pm 0.008)I + (1.15 \pm 0.192). \quad (5)$$

For the red GC subpopulation:

$$(V - I)_0 = (0.011 \pm 0.013)I + (0.88 \pm 0.299). \quad (6)$$

The GC system of NGC 1272 also exhibits red and blue subpopulations, with the blue subpopulation exhibiting a blue tilt, with the slope of the fit to the red subpopulation exhibiting a slope consistent with zero within the errors. Similar to NGC 1275, the UCDs in the vicinity of NGC 1272 occupy the bright end of the CMD, falling on both the blue and red subpopulations. This further strengthens the argument for UCDs being an extension of the GC population to larger sizes.

As for NGC 1275, we investigate radial colour trends in the GC colours by examining the colours of the galaxy’s GC system versus distance from the galaxy centre. We examine the GC system of this galaxy out to $R = 50$ kpc, which is the approximate midpoint of the projected distance between NGC 1272 and its nearest neighbouring massive elliptical to avoid confusion between the two galaxies GC systems. Unlike NGC 1275, we cannot distinguish the two subpopulations in this radial colour distribution, with a fit to the GC system as a whole given by

$$(V - I)_0 = (-0.0029 \pm 0.0005)D + (0.988 \pm 0.0117), \quad (7)$$

where D is the distance from the galaxy centre in kpc.

The colours of the galaxy's GC system become increasingly bluer with galactocentric distance. However, this may simply reflect the changing mix of GC subpopulations with galactocentric distance, such that the blue subpopulation extends to larger radii than the red subpopulation.

6 DISCUSSION

We have identified a large population of 84 UCD candidates out to 250 kpc distance from the Perseus cluster-centred galaxy NGC 1275. The colours of these UCDs are, in general, consistent with old, passive stellar populations, lying on an extrapolation of the dE CMR to fainter magnitudes. Furthermore, Perseus dE nuclei and UCDs have very similar colours, in agreement with the results of Brodie et al. (2011). This result suggests a possible evolutionary link between UCDs and dE nuclei. However, UCDs also show similarities to GCs in terms of their colour distribution, such that they lie on the bright ends of the blue and red GC subpopulations.

In terms of size–luminosity trends, we confirm the findings of Brodie et al. (2011) that UCDs occupy a broad locus in size–luminosity parameter space. A size–luminosity trend is seen for the Perseus UCDs, in that the largest UCDs have the highest luminosities, but at fainter magnitudes (M_V fainter than -12), the spread in the distribution of UCD sizes at a given magnitude is large, such that these objects do not show a well-defined size–luminosity relation.

We identify in our sample a number of ‘extended’ UCDs with sizes between 30 and 57 pc. Gilmore et al. (2007) suggest that star clusters have characteristic sizes <30 pc, whereas all larger galaxies are galaxies with sizes >120 pc, with no objects having sizes $30 < r_e < 120$ pc. This result is not in agreement with the sizes of the more extended UCDs we identify in Perseus. Our size measurements are complimented by those of Brodie et al. (2011) who find examples of such objects in Virgo with spectroscopically confirmed redshifts, further blurring the boundary between massive star clusters and compact galaxies. Although the nature of UCDs remains unknown, they are filling the scale-size gap between galaxies and star clusters proposed in Gilmore et al. (2007).

One possible formation scenario for the Perseus UCD population is that they are an extension of the GC system to brighter magnitudes. This is discussed in more detail below. We also discuss two alternative formation scenarios for these objects: they are the remnants of nucleated dEs that have been tidally stripped by massive galaxies and the cluster potential; or they are formed in the star-forming regions of the filaments surrounding NGC 1275.

6.1 UCDs as massive globular clusters

The Perseus UCD and GC populations both follow the same radial surface distributions at distances $D > 30$ kpc from NGC 1275 (Fig. 6), suggesting they are part of the same distribution. At smaller galactocentric distances, the radial surface density of UCDs flattens off, suggesting these objects are either disrupted at small distances, or cannot form in the increased tidal potential of their host galaxy.

The UCDs in the vicinity of NGC 1275 and NGC 1272 follow the same colour–magnitude trend as the GC systems of these galaxies, such that there are blue and red subpopulations of Perseus UCDs. Around NGC 1275, there is also evidence that a fraction of UCDs follow the colour–distance trend of the GC population, such that bluer objects are found at larger projected radii from the massive galaxy. These similarities suggest that some UCDs in Perseus might be massive GCs.

We find UCDs to be consistent with the colour–magnitude trend of dEs to fainter magnitudes and blue GCs to higher magnitudes. So unlike Brodie et al. (2011) we did not find evidence for the UCDs to be offset (to bluer colours at a given magnitude) compared to the blue GCs. However we note that our overlapping magnitudes for both UCDs and GCs are small.

6.2 UCDs as tidally stripped of nuclei dwarf ellipticals

The colours of Perseus UCDs are also remarkably similar to those of dE nuclei, similar to the findings of Brodie et al. (2011). One formation mechanism for UCDs is through the tidal stripping of nucleated dEs (Bekki et al. 2001; Drinkwater et al. 2003). UCDs have been observed to have a range of α enhancements (Brodie et al. 2011). This is also consistent with dEs, which are known not to be a simple, homogeneous population, but rather exhibit a range of ages and metallicities inconsistent with a single formation scenario (Penny & Conselice 2008). We therefore consider the possibility that dE nuclei are the progenitors of UCDs by considering the Perseus dE population.

The faint-end slope of the luminosity function in Perseus is remarkably shallow at $\alpha = -1.26$ (Penny & Conselice 2008), suggesting the core of Perseus may be dwarf depleted. The destruction of dEs via tidal processes is once such way to explain this shallow faint-end slope. Nucleated dEs are abundant in Perseus, and such galaxies have been suggested as the progenitors of UCDs (Bekki et al. 2001; Drinkwater et al. 2003). Furthermore, cD/BCG galaxies likely reach their large masses via numerous mergers and tidal interactions with other cluster members (e.g. Brough et al. 2011). The low-density outer regions of nucleated dEs would be easily stripped, with the more compact nuclei left behind. Very deep imaging to extremely low surface brightness ($\mu_V = 29$ mag arcsec $^{-2}$) is required to search for the tidal debris that would result from the stripping of the stellar light envelopes of nucleated dEs.

Using the technique of Penny et al. (2009), we can estimate how close a typical nucleated dE must come to the cluster centre for stars at its visible (Petrosian) radius to be stripped by the cluster potential. By estimating the strength of the tidal potential acting on a star located at the Petrosian radius of the dwarf, we can estimate how massive the dwarf must be to prevent its disruption by the tidal potential (or host galaxy). We calculate this for a typical dE of size $r_e = 1.5$ kpc and mass $10^8 M_\odot$. This dwarf is dE 10 from Conselice, Gallagher & Wyse (2003), and is located at a projected distance of 193 kpc from NGC 1275.

Fig. 18 shows that at distances <100 kpc from the cluster centre, a typical nucleated dE will not have enough visible mass to retain stars in its outer region. Therefore, it is plausible that a number of the UCDs we see in clusters today are the remnant nuclei of dEs that did not reside in sufficiently massive dark matter haloes to prevent their tidal disruption. Nucleated dEs would therefore be easily stripped of their outer stellar envelopes via tidal processes, with only their dense nuclei, that have sizes similar to UCDs, remaining to the present day. The fact that number density of UCDs is flat in the inner regions of NGC 1275 (Fig. 6) does not necessarily rule out a galaxy stripping origin for UCDs. If tidal forces are sufficiently strong in the inner regions of the galaxy, more extended clusters or nuclei will be stripped to smaller radii by tidal effects.

The $H\alpha$ filaments present in the deeper R -band imaging make searching for tidal structures that would indicate tidal interactions at small galactocentric distances difficult. The B -band imaging is free of these filamentary structures, and exhibits faint shells, indicating that galaxy–galaxy interactions have taken place here. NGC 1275

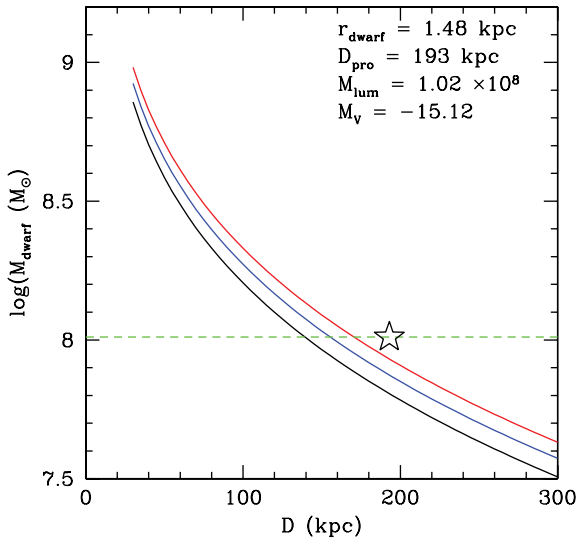


Figure 18. The minimum stellar mass a nucleated dE must have to prevent stars at the Petrosian radius of the dwarf being stripped by the cluster potential as a function of clustercentric distance. The three lines represent (from bottom to top) orbital eccentricities of 0, 0.5 and 1. These masses were calculated using the method of Penny et al. (2009) for a Perseus nucleated dE of size 1.5 kpc, located at 03:19:00, +41:29:02 (dE 10 in Conselice et al. 2003). The stellar mass of the dE in this example is $10^8 M_{\odot}$. The green dashed line is the stellar mass of the dwarf, and the star is located at its current projected distance from the cluster centre (193 kpc). At small distances from the cluster centre (<140 kpc), a typical nucleated dE will be easily stripped of its outer stars unless it has a large enough dark matter mass to prevent this.

is a shell galaxy (Holtzman et al. 1992; Conselice, Gallagher & Wyse 2001), with these shells formed via the accretion of satellite galaxies which contribute to the mass build up of the BCG.

To highlight these shells, we perform an unsharp mask subtraction on this imaging. Features are highlighted by dividing the original image by a smoothed version of itself. The image was filtered using a 300×300 pixel median filter using IRAF IMFILTER. The original image was then divided by the filtered image to remove large-scale structure (such as galaxy light), with smaller scale features such as shells and dust lanes remaining. The result of this subtraction is shown in Fig. 19. Numerous low surface brightness shells are visible in this imaging, with the brightest shells located towards the centre of the galaxy, with fainter shells visible at larger radii.

Such interactions would disrupt the diffuse stellar envelopes of dEs more easily than their dense nuclei. While the remnants from such interactions would be impossible to detect in our existing imaging due to their extremely low surface brightness, nevertheless tidal interactions likely play an important role in the cluster core.

The majority of nucleated dwarfs in Perseus are very smooth, round systems, with no evidence for asymmetry in their structures that would indicate interactions with the cluster tidal potential (Penny et al. 2009). However, these may just be the dEs that are dark matter dominated enough to survive unperturbed to the present day. A fraction of the UCD population of Perseus may therefore be the remnants of stripped dEs.

6.3 UCD formation in filaments

Given the proximity of NGC 1275 UCDs to the gaseous filaments surrounding this galaxy, we investigate these filaments as a possible site for UCD formation. NGC 1275 is an unusual galaxy, and

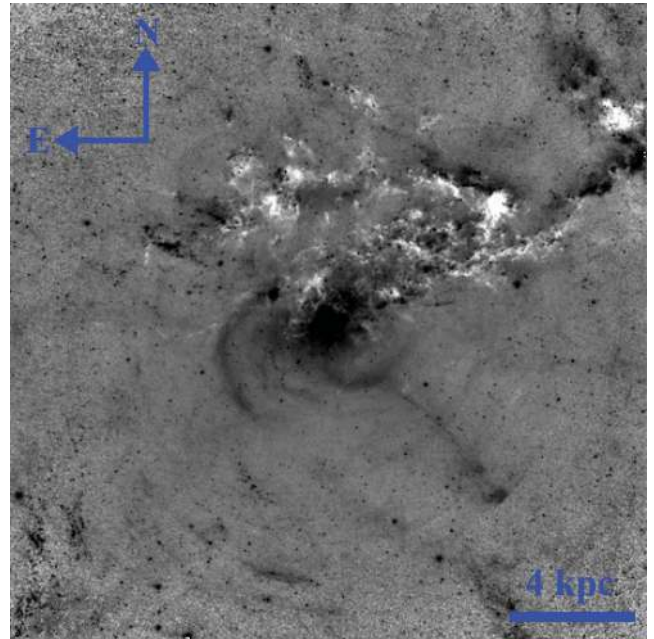


Figure 19. The shells around NGC 1275 highlighting low surface brightness features in the galaxy’s halo. This image was created by dividing the original image by a smoothed version of itself to highlight fine structures. Several shells can be seen to the top right-hand side of the galaxy, with a long plume-like structure intersecting the shells. These shells indicate that past galaxy–galaxy interactions have taken place in this region of the cluster core. The patchy dust to the north of the image belongs to the foreground high-velocity system.

likely represents a good analogue for processes that occurred at higher z for brightest cluster/group galaxies, as it is still actively undergoing formation and evolution. NGC 1275 exhibits a highly complex structure (Fig. 20), surrounded by a complex system of $H\alpha$ filaments.

A number of the filaments surrounding NGC 1275 are associated with active star formation. Such star-forming regions are likely formed when cooling gas collapses into thinner filaments, leading to star formation (McDonald et al. 2010). A similar region of star formation to those observed around NGC 1275 has been observed in Abell 1795, but otherwise remain essentially unstudied. This suggests that such filamentary star-forming structures are relatively short lived, with supernova feedback rapidly removing the material for further star formation in these structures. If such star-forming filamentary structure were more common at higher z , this would naturally explain the old ages seen for the majority of UCDs.

The number of UCD candidates we identify in the vicinity of NGC 1275 could therefore be due to their formation in the cluster-centred galaxy. Massive compact blue star clusters are known to exist in the core of NGC 1275, which have been hypothesized to be proto-GCs with masses 10^7 – $10^8 M_{\odot}$ (Brodie et al. 1998). However, star formation is not limited to the core of the BCG, but rather extends to a number of knots and loops of star-forming regions that enshroud the galaxy. The mechanisms for star formation in these regions has already been discussed in detail elsewhere (e.g. Canning et al. 2010) so will not be examined further in this work. Given that star formation is actively ongoing in this massive galaxy, this may provide a source of new UCDs in the cluster.

The star-forming filaments contain numerous young, massive star clusters. Canning et al. (2010) estimate typical masses for the brightest star clusters of $10^7 M_{\odot}$, with the typical UCD masses

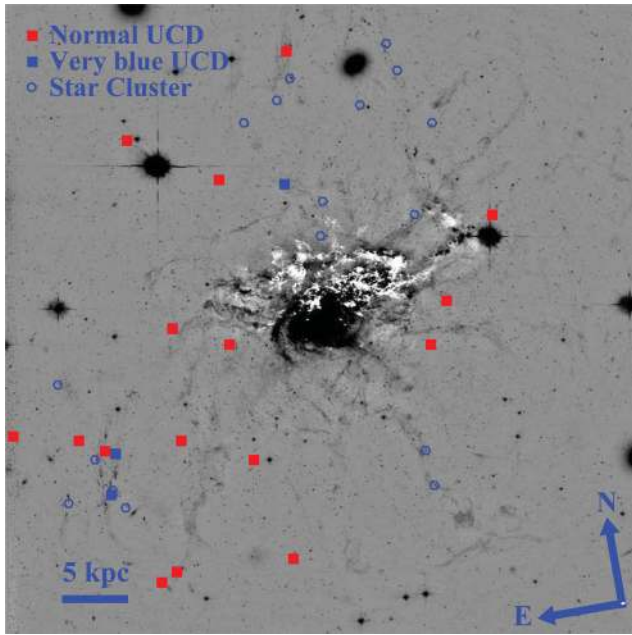


Figure 20. An unsharp mask subtracted image of the *F625W* imaging of NGC 1275. This image highlights the complex system of filaments that surround the galaxy. Overplotted on the image are the positions of the UCDs within this field of view. The blue filled squares are those UCDs that have colours $(B - R)_0 < 0.6$. The red filled squares are UCDs with typical colours. The blue open hexagons are objects with round morphologies reminiscent of GCs/UCDs and $S/N > 40$, but without reliable size measurement as they reside in crowded regions.

being 10^6 – $10^8 M_\odot$ (Mieske et al. 2008). Through mergers, these young, massive star clusters build up enough mass to obtain sizes and luminosities consistent with those of the most massive UCDs. The very blue UCDs are likely early on in their formation, before their stellar populations have aged enough to resemble those of normal UCDs identified in previous studies.

The three very blue UCDs we identify are all located in the vicinity of NGC 1275, with ‘normal’ UCDs distributed more evenly through the cluster (Fig. 14). Given the young ages of their stellar populations (< 0.1 Gyr), they must have formed very recently, and will therefore will not have had enough time to migrate away from their formation site. This strongly suggests that the young, proto-UCDs are linked to the ongoing star formation in the filaments. Perturbations by other cluster galaxies provide a mechanism to distribute these objects through the cluster.

A sequence of young, very blue objects with $(B - R)_0 < 0.5$ are seen in the colour–magnitude diagram around NGC 1275 (Fig. 2). A number of these blue star clusters are in regions that are too crowded for accurate size determination, along with more isolated young, blue GC-sized objects. Further examples of proto-UCDs therefore exist in the vicinity of NGC 1275. The locations of these very blue, round objects, along with UCDs in the immediate vicinity of NGC 1275 are shown on an *R*-band unsharp mask image in Fig. 20. These objects are all located on or near filaments, hinting these are their formation sites.

The typical colour of a UCD is $(B - R)_0 \sim 1.3$, which corresponds to an age of ~ 1 Gyr for its stellar population. Canning et al. (2010) argue that at least some of the star clusters in these regions of star formation are being tidally disrupted by their host galaxy due to their elongated structures. If this is the case, a low-mass star cluster might not withstand the tidal forces of the host galaxy long enough

for its colours to transform to those typical for a UCD. Through mergers, young, blue star clusters could reach a sufficient mass such that they are able to survive the tidal forces of NGC 1275 to the present day to appear as UCDs in the clusters. However, individual star clusters within the filaments are remarkably round, with ellipticity ~ 1 , showing they are already of sufficient mass to prevent tidal stripping and elongation by their host potential. A high-mass, compact structure would be robust against the tidal forces in the cluster core, unlike the diffuse envelopes of dEs. Those with $(B - R)_0 \sim 0.5$ must already have survived 100 Myr without disruption, therefore, the more massive UCD/GC sized objects in these filaments are resilient against such tidal interactions.

To investigate this UCD formation mechanism, it will be necessary to investigate other clusters or groups that exhibit filamentary structure in the nearby (100 Mpc) Universe. If young, blue UCDs are seen, this would strengthen the hypothesis that such objects are formed in these filaments. These young, very blue UCDs furthermore highlight the importance of utilizing a complete range of colours ranging from star forming to passive when carrying out searches for such objects.

7 CONCLUSIONS

We identify in the Perseus cluster core 84 UCD candidates. The majority of these objects have sizes and colours that are comparable with those of UCDs identified in previous studies. Three UCD-sized objects are bluer than typical UCDs, exhibiting $(B - R)_0$ colours of 0.28, 0.54 and 0.59. These colours are consistent with objects that have ceased star formation in the last 100 Myr, and are therefore still located close to their formation site. The very blue UCDs are at projected distances < 25 kpc from the centre of NGC 1275, and are furthermore located near the star-forming filaments that surround the galaxy. Numerous other large, round star clusters in star-forming filaments too crowded for accurate size determination are also seen.

Based on these objects, and the fact that UCDs in Perseus are remarkably centrally concentrated around the BCG NGC 1275, we hypothesize that a fraction of the UCD population are formed in the star-forming filaments surrounding this galaxy. Through mergers, massive star clusters in these regions are able to reach the masses and sizes typically seen for UCDs. Many star clusters within these filaments have colours of $(B - R)_0 \sim 0.5$, consistent with stellar populations of age ~ 100 Myr. These star clusters therefore must be robust against tidal perturbations to survive for sufficient time-scales that their stellar populations become red. Over time, such objects will become more evenly distributed through the cluster due to perturbations from other cluster galaxies.

We do not rule out other UCD formation mechanisms such as tidal stripping or massive GCs, based on similarities between UCDs and both dE nuclei and GCs. UCDs and GCs share a similar radial density profile, implying they are part of the same population. Numerous faint tidal features and shells are visible around NGC 1275, providing evidence that at least some of the UCDs in Perseus were formed by such tidal interactions.

We compared the colours of the Perseus UCDs to GC systems of NGC 1275 and NGC 1272 to investigate if UCDs are massive GCs. UCDs also lie on the bright end of the GC colour–magnitude trend, following the blue and red subpopulations, suggesting they may be a bright extension of the GCs. It is therefore likely that a number of formation scenarios are required to explain the origin of UCDs in the cluster environment, strengthening the argument that UCDs are not a simple class of objects (cf. Norris & Kannappan 2011). We therefore conclude that although the Perseus cluster is

an ideal environment to strip nucleated dE and hence form UCDS, we cannot easily discriminate that origin from a massive star cluster one. Neither can we rule out a new formation path within gaseous filaments.

ACKNOWLEDGMENTS

We thank the anonymous referee for their comments that helped improve this paper. SJP acknowledges the support of a DEEWR Endeavour Post-doctoral Award and an ARC Super Science Fellowship. CJC acknowledges support from the STFC and the Leverhulme Trust. This research has made use of the NASA/IPAC Extragalactic Database (NED) which is operated by the Jet Propulsion Laboratory, California Institute of Technology, under contract with the National Aeronautics and Space Administration. Some of the data presented in this paper were obtained from the Multimission Archive at the Space Telescope Science Institute (MAST). STScI is operated by the Association of Universities for Research in Astronomy, Inc., under NASA contract NAS5-26555. Support for MAST for non-*HST* data is provided by the NASA Office of Space Science via grant NNX09AF08G and by other grants and contracts.

REFERENCES

- Bekki K., Couch W. J., Drinkwater M. J., 2001, *ApJ*, 552, L105
- Bertin E., Arnouts S., 1996, *A&AS*, 117, 393
- Brodie J. P., Schroder L. L., Huchra J. P., Phillips A. C., Kissler-Patig M., Forbes D. A., 1998, *AJ*, 116, 691
- Brodie J. P., Romanowsky A. J., Strader J., Forbes D. A., 2011, *AJ*, 142, 199
- Brough S., Tran K.-V., Sharp R. G., von der Linden A., Couch W. J., 2011, *MNRAS*, 414, L80
- Brüns R. C., Kroupa P., Fellhauer M., Metz M., Assmann P., 2011, *A&A*, 529, A138
- Bruzual G., Charlot S., 2003, *MNRAS*, 344, 1000
- Burstein D., Heiles C., 1984, *ApJS*, 54, 33
- Canning R. E. A., Fabian A. C., Johnstone R. M., Sanders J. S., Conselice C. J., Crawford C. S., Gallagher J. S., Zweibel E., 2010, *MNRAS*, 405, 115
- Chiboucas K. et al., 2011, *ApJ*, 737, 86
- Conselice C. J., Gallagher J. S., III, Wyse R. F. G., 2001, *AJ*, 122, 2281
- Conselice C. J., Gallagher J. S., III, Wyse R. F. G., 2003, *AJ*, 125, 66
- de Rijcke S., Penny S. J., Conselice C. J., Valcke S., Held E. V., 2009, *MNRAS*, 393, 798
- de Vaucouleurs G., de Vaucouleurs A., Corwin H. G., Jr, Buta R. J., Paturel G., Fouque P., 1991, *Third Reference Catalogue of Bright Galaxies*. Springer-Verlag, Berlin
- Drinkwater M. J., Jones J. B., Gregg M. D., Phillipps S., 2000, *Publ. Astron. Soc. Australia*, 17, 227
- Drinkwater M. J., Gregg M. D., Hilker M., Bekki K., Couch W. J., Ferguson H. C., Jones J. B., Phillipps S., 2003, *Nat*, 423, 519
- Evstigneeva E. A., Gregg M. D., Drinkwater M. J., Hilker M., 2007, *AJ*, 133, 1722
- Evstigneeva E. A. et al., 2008, *AJ*, 136, 461
- Fellhauer M., Kroupa P., 2002, *MNRAS*, 330, 642
- Forbes D. A., Kroupa P., 2011, *Publ. Astron. Soc. Australia*, 28, 77
- Forbes D. A., Spitler L. R., Strader J., Romanowsky A. J., Brodie J. P., Foster C., 2011, *MNRAS*, 413, 2943
- Fukugita M., Shimasaku K., Ichikawa T., 1995, *PASP*, 107, 945
- Gilmore G., Wilkinson M. I., Wyse R. F. G., Kleyna J. T., Koch A., Evans N. W., Grebel E. K., 2007, *ApJ*, 663, 948
- Graham A. W., Guzmán R., 2003, *AJ*, 125, 2936
- Grebel E. K., Gallagher J. S., III, Harbeck D., 2003, *AJ*, 125, 1926
- Gregg M. D. et al., 2009, *AJ*, 137, 498
- Harris W. E., 2009, *ApJ*, 699, 254
- Harris W. E., Kavelaars J. J., Hanes D. A., Pritchett C. J., Baum W. A., 2009, *AJ*, 137, 3314
- Haşegan M. et al., 2005, *ApJ*, 627, 203
- Hilker M., Infante L., Vieira G., Kissler-Patig M., Richtler T., 1999, *A&AS*, 134, 75
- Holtzman J. A. et al., 1992, *AJ*, 103, 691
- Huxor A. P., Phillipps S., Price J., Harniman R., 2011, *MNRAS*, 414, 3557
- Kent S. M., 1987, *AJ*, 94, 306
- Kissler-Patig M., Jordán A., Bastian N., 2006, *A&A*, 448, 1031
- Larsen S. S., 1999, *A&AS*, 139, 393
- McDonald M., Veileux S., Rupke D. S. N., Mushotzky R., 2010, *ApJ*, 721, 1262
- Madrid J. P. et al., 2010, *ApJ*, 722, 1707
- Martin N. F., de Jong J. T. A., Rix H.-W., 2008, *ApJ*, 684, 1075
- Mieske S. et al., 2008, *A&A*, 487, 921
- Mieske S., Hilker M., Misgeld I., Jordán A., Infante L., Kissler-Patig M., 2009, *A&A*, 498, 705
- Minkowski R., 1955, in van de Hulst H. C., ed., *Proc. IAU Symp. 4, Radio Astronomy*. Cambridge Univ. Press, Cambridge, p. 107
- Misgeld I., Hilker M., 2011, *MNRAS*, 414, 3699
- Misgeld I., Mieske S., Hilker M., 2008, *A&A*, 486, 697
- Misgeld I., Hilker M., Mieske S., 2009, *VizieR Online Data Catalog*, 349, 60683
- Misgeld I., Mieske S., Hilker M., Richtler T., Georgiev I. Y., Schuberth Y., 2011, *A&A*, 531, A4
- Norris M. A., Kannappan S. J., 2011, *MNRAS*, 414, 739
- Penny S. J., Conselice C. J., 2008, *MNRAS*, 383, 247
- Penny S. J., Conselice C. J., de Rijcke S., Held E. V., 2009, *MNRAS*, 393, 1054
- Price J. et al., 2009, *MNRAS*, 397, 1816
- Schlegel D. J., Finkbeiner D. P., Davis M., 1998, *ApJ*, 500, 525
- Sirianni M. et al., 2005, *PASP*, 117, 1049
- Smith Castelli A. V., Faifer F. R., Richtler T., Bassino L. P., 2008, *MNRAS*, 391, 685
- Strader J., Smith G. H., 2008, *AJ*, 136, 1828
- Struble M. F., Rood H. J., 1999, *ApJS*, 125, 35
- Wehner E. M. H., Harris W. E., Whitmore B. C., Rothberg B., Woodley K. A., 2008, *ApJ*, 681, 1233

This paper has been typeset from a $\text{\TeX}/\text{\LaTeX}$ file prepared by the author.